This article has been accepted for publication in IEEE Open Journal of the Communications Society. This is the author's version which has not been fully edited and content may change prior to final publication. Citation information: DOI 10.1109/OJCOMS.2025.3552727

Received XX Month, XXXX; revised XX Month, XXXX; accepted XX Month, XXXX; Date of publication XX Month, XXXX; date of current version XX July, 2024.

Digital Object Identifier 10.1109/OJCOMS.2024.011100

Full-Duplex Techniques for Satellite Communications: Feasibility Analysis and Roadmap

Eva Lagunas[1] *(Senior Member, IEEE)*, Tomas Ramirez-Parracho[3], Juan Andres Vasquez-Peralvo[1] *(Senior Member, IEEE)*, Jorge Luis Gonzalez-Rios[1] *(Member, IEEE)*, Pablo Losada[3], Carlos Mosquera[2] *(Senior Member, IEEE)*, Roberto López-Valcarce[2] *(Senior Member, IEEE)*, Praveen Naidu Vummadisetty[1] *(Senior Member, IEEE)*, Symeon Chatzinotas[1] *(Fellow Member, IEEE)*

[1]Interdisciplinary Centre for Security Reliability and Trust (SnT), University of Luxembourg, Luxembourg
[2]atlanTTic Research Center, Universidade de Vigo, Spain
[3]Gradiant, Vigo, Spain

CORRESPONDING AUTHOR: Eva Lagunas (e-mail: eva.lagunas@uni.lu).

This work has been supported by European Space Agency (ESA) funded activity FDSat: Single Channel Full Duplex Techniques for Satellite Communications (4000140117/22/NL/CLP). The views of the authors of this paper do not necessarily reflect the views of ESA.

ABSTRACT The non-terrestrial communication industry is required to optimize the use of the available radio frequency (RF) spectrum and, in turn, lower the cost per delivered bit. Full-Duplex (FD) is a widely studied technology in the terrestrial domain, which allows the data transmission simultaneously in both directions of the same frequency channel. In this work, we study and evaluate the feasibility of using FD techniques within SatCom networks. First, a survey of the current state of the art for self-interference cancellation (SIC) techniques and technology is presented, to set the baseline of achievable interference cancellation with currently available technology. Subsequently, different SatCom use cases are identified, including different satellite orbits and types of links, and a detailed feasibility evaluation is carried out through analytical models and simulations. The most promising scenarios are shown to be both LEO feeder and downlink in Q/V and Ka band, respectively, and an on-ground FD between terrestrial and satellite backhauling in Ka-band. To conclude, we identify the technological shortcomings and outline a possible roadmap for developing and implementing the necessary self-interference cancellation methods to facilitate FD communications in the selected use cases.

INDEX TERMS Full-duplex, satellite communications, spectral efficiency, self-interference cancellation

I. INTRODUCTION

MOST satellite communication (SatCom) systems operate in a half-duplex fashion, where two separate frequency channels are used to ensure perfect isolation between the transmitted and received signal. As data volume demands continue to rise, along with the pressure to lower the cost per bit delivered, there is an ongoing need for new techniques to make more efficient use of the available radio frequency (RF) spectrum.

Full-Duplex (FD) operation refers to the simultaneous transmission and reception of information, either within a single (in-band) channel or across very close frequency channels. FD has demonstrated promising results in the terrestrial wireless domain, e.g. [1], [2]. Between 2010 and 2020, FD technology has advanced significantly, transitioning from a conceptual laboratory idea to being integrated into certain telecommunications standards. Driven by the promising results seen in terrestrial wireless communication, the ESA project FDSat, ”Single Channel Full Duplex Techniques for Satellite Communications,” [3] was initiated to examine the unique challenges of implementing FD in SatCom scenarios.

Orthogonal frequency separation is typically employed in SatCom systems to achieve interference-free bidirectional communication links, with proper spectral filtering (Frequency Division Duplexing, FDD). Thus, one has a user equipment (UE)-to-satellite-to-ground link (uplink) and a

This work is licensed under a Creative Commons Attribution 4.0 License. For more information, see https://creativecommons.org/licenses/by/4.0/

This work is licensed under a Creative Commons Attribution 4.0 License. For more information, see https://creativecommons.org/licenses/by/4.0/

This article has been accepted for publication in IEEE Open Journal of the Communications Society. This is the author's version which has not been fully edited and content may change prior to final publication. Citation information: DOI 10.1109/OJCOMS.2025.3552727

ground-to-satellite-to-UE link (downlink), which are multiplexed in different frequency bands. Furthermore, conventional SatCom systems consider a transparent payload, so that received signals are simply amplified and converted to a different frequency.

Single-channel bi-directional communication may also be implemented by Time Division Duplexing (TDD), but is rarely used in SatCom systems, e.g., the Iridium user and inter-satellite links. In both cases, the gains of switching to FD operation are attractive, with the potential not only to double the spectral efficiency in the case of in-band FD (IBFD), but also to reduce communication latency with respect to TDD. However, FD also introduces the problem of self-interference (SI), as the signal from the transmitter (TX) leaks into the receiver (RX), which becomes desensitized, and corrupts the signal of interest.

SatComs have certain characteristics that make FD operation particularly challenging when compared to that of the terrestrial counterpart. One key factor is the significant power imbalance between the transmitted and received signals. Due to the long propagation distance (e.g. ∼36,000 km for GEO satellites and between 500-1300 km for LEO satellites), the TX power is very strong while the RX signal is very attenuated. Such imbalance between TX and RX power poses serious difficulties at the self-interference cancellation (SIC) process. Furthermore, neither the user equipment (UE) nor the satellite payload can support sophisticated hardware components, as they shall keep cost, mass and volume within strict limits. In addition, satellite channels generally consider wide bandwidths and high operational frequencies, which makes the signal processing for SIC particularly demanding.

The focus of this work is to assess the required level of SIC that is needed to achieve a given performance level with the use of IBFD operation. SIC is the key figure of merit to assess IBFD feasibility, which is the reason why our focus is on SIC and not on other types of co-channel interference. IBFD systems generally utilize a blend of analog and digital SIC strategies, in addition to careful antenna design and placement, to obtain the necessary isolation between transmitted and received signals.

The remainder of the paper is organized as follows. In Sec. II we first review the basics of FD operation to later examine the most relevant works related to SIC, as well as briefly discuss standardization activities. Sec. III focuses on SatCom FD use cases and provides the relevant parametrization of each use case as well as the typical link budget for a common half-duplex (HD) operation. Sec. IV presents an initial feasibility analysis of FD operation, with a shortlisting of promising use cases based not only on technical feasibility but also from a practical and business-oriented point of view. Sec. V presents a discussion on alternatives for antenna passive isolation, and in Sec. VI a detailed analysis of the selected use cases considering hardware imperfections is given. The paper concludes in Sec. VII with a discussion of technological gaps and FD-SatCom roadmap, with a focus on the most promising emerging technologies.

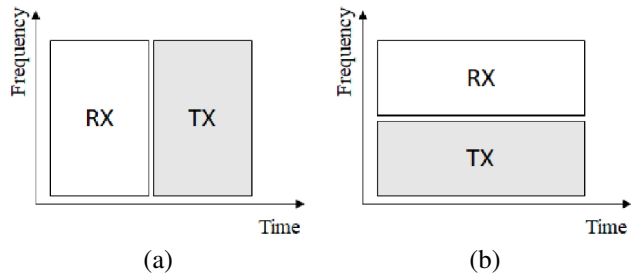

FIGURE 1. **Half-Duplex operation mode: (a) TDD, (b) FDD.**

II. State-of-the-Art

A. Conventional Duplexing Modes: Half-Duplex

Conventional wireless network design has been based on HD operation, according to which a node either transmits or receives in a single channel use [1]. HD designs are typically based either on TDD, illustrated in Fig. 1(a), or in FDD, as shown in Fig. 1(b).

TDD shows some benefits when compared with FDD [4], as it allows to dynamically assign time resources to uplink (UL) and downlink (DL) depending on the expected traffic volume of each direction. In this case, DL typically gets more time resources assigned due to the significantly higher DL traffic compared to the UL. In addition, channel reciprocity can be exploited in TDD to obtain the channel state information (CSI), eliminating the need to estimate the channel in both directions, thus reducing the related overhead. On the downside, there exists a time gap between DL reception and UL transmission in TDD, which is unavoidably longer than that in FDD, resulting in acknowledgment feedback delay. For the same reason, TDD entails a latency in the communication which is absent in FDD systems. In addition, tight network synchronization is needed in TDD mode to make sure that DL and UL segments from different transmissions do not overlap. This is especially critical in SatCom systems due to the long propagation delay differentials.

B. Full-Duplex Operation Essentials

FD has attracted significant attention as en effective way to increase the spectral efficiency. As discussed in [5], the simultaneous transmission and reception operations over the same frequency band (i.e., IBFD operation) provides the potential benefit of doubling spectral efficiency (information bits that can be communicated per second and per Hz), and therefore might represent a significant breakthrough for next-generation wireless networks.

Initial results with off-the-shelf radios in 2010 evidenced the possibility to consider practical IBFD [6], [7], but still showed the challenge posed by high SI levels. Accurate SI cancellation was found to be instrumental for IBFD operation and, more generally, for other FD settings With considerable

This work is licensed under a Creative Commons Attribution 4.0 License. For more information, see https://creativecommons.org/licenses/by/4.0/

This article has been accepted for publication in IEEE Open Journal of the Communications Society. This is the author's version which has not been fully edited and content may change prior to final publication. Citation information: DOI 10.1109/OJCOMS.2025.3552727

signal leakage from the transmit antenna into the reception chain, including Out-of-Band Full-Duplex (OBFD). In the literature, OBFD is sometimes regarded as HD FDD with reduced guard bands. The different FD modes are illustrated in Fig. 2.

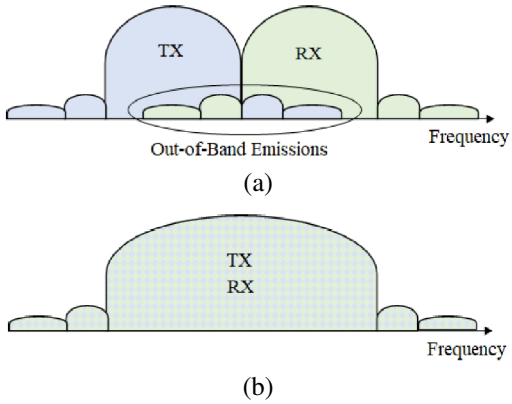

FIGURE 2. Different FD modes: (a) Out-of-Band Full-Duplex (OBFD), similar to HD FDD, (b) In-Band Full-Duplex (IBFD).

C. Recent works on FD operation

The recent special issue published in [8] confirms the potential of FD to be part of future wireless standards. The purpose of the present work is not to provide a complete survey on FD works but rather to present the basics and latest results, with a focus on application to the SatCom domain.

1) Self-Interference Cancellation

For a successful IBFD operation, the transceiver must suppress SI to an acceptable level [9]. In particular, a signal-to-noise ratio (SNR) degradation of less than 1 dB is achieved if the SI is set to be 6 dB (or more) below the receiver noise floor. In such case, close to $\times 2$ spectral efficiency gain can be achieved with respect to the two-way radio link. SIC techniques should capture all different sources of distortion affecting the SI signal, from its origin at the transmission chain and up to the RX end. Conceptually, the SI signal is often split into different parts: linear and non-linear components, and thermal noise [10]. From the perspective of FD operation, the degradation in performance with respect to HD resides in the limited capability of the SIC processing subsystem to faithfully replicate the aforementioned SI components.

SIC techniques can be broadly categorized as either *passive* or *active*. Pasive approaches, also known as propagation domain techniques, are based on careful antenna and/or circulator designs, antenna placement, the inclusion of absorbers or electromagnetic shielding (also known as spatial duplexer [11]), or the use of cross-polarization, among others [10], [12], [13]. Active techniques attempt to synthesize a replica of the SI and then substract it from the received signal; this can be done in the analog (RF) domain, in the digital (baseband) domain, or using a combination of both [10], [14], [15].

Thus, the mitigation of the linear SI component can be addressed in either of these domains. This task can be challenging depending on the structure of the effective SI channel. SI channel responses comprising multiple echos spread over a long time interval will require more complexity in the SIC process. However, not all echos may need to be suppressed, and a trade-off between suppression accuracy and complexity can be devised for a target SIC suppression level. SI channel models are often derived from empirical characterizations of the SI channel observed by the radiating elements of a given system when deployed in a controlled environment or in the field. The non-linear SI component includes distortion produced by amplifiers, phase noise, quantization noise, and I/Q imbalances, and is generally more difficult to address; if feasible, some cases might require additional linearization in the form of pre-distortion to limit the impact of SI.

In [16], it was shown that 30 dB is usually the maximum it can be achieved with active analog SI cancellation, although as much as 45 dB have been reported with realistic system configurations and wideband signals [17]. The practical feasibility of these solutions has been questioned by several companies in the realm of 3GPP discussions on full-duplex technology, due to the complexity of interconnections between all TX and RX elements in the case of panel arrays, as well as the associated losses and the increase in size and weight [18].

Active digital SI cancellation performance is very sensitive to the non-ideal characteristics of the transceiver, mainly the nonlinearity of the power amplifier (PA) at the TX, but also the I-Q imbalance of the up- and down-converters, as well as nonlinearities introduced by the Low Noise Amplifier (LNA) at the RX. For multiantenna systems, complexity can be very high due to the large number of TX-RX combinations. For single-antenna transceivers, some reference values have been given in [19], which reports 30 dB of digital SIC over a 16-MHz bandwidth; in [20], which provides insights on the digital cancellation performance for the DoubleTalk® system, with up to 30 dB of digital SIC in the absence of significant signal impairments and over an unspecified bandwidth; and in [10, Ch. 11], reporting 40-45 dB depending on the bandwidth (between 20 and 80 MHz) and under limited nonlinear impairments.

From the point of view of passive SIC techniques, three main antenna architectures may be considered regarding FD operation, namely the separate-antenna (i.e., bi-static) architecture, the single-antenna (i.e., monostatic) architecture, and phased arrays. In the separate-antenna architecture, both TX and RX chains use a dedicated antenna each, whereas in the single-antenna configuration, they share a common antenna by means of some appropriate interface (e.g., circulator, balanced duplexer, etc. [10], [21]). Although

This work is licensed under a Creative Commons Attribution 4.0 License. For more information, see https://creativecommons.org/licenses/by/4.0/

This article has been accepted for publication in IEEE Open Journal of the Communications Society. This is the author's version which has not been fully edited and content may change prior to final publication. Citation information: DOI 10.1109/OJCOMS.2025.3552727

the single-antenna architecture is simpler from the hardware perspective, it usually yields lower isolation than the separate-antenna configuration, which provides additional degrees of freedom for passive SIC design. However, having separate antenna elements is not always possible due to real estate constraints. Last but not least, antenna arrays with beamforming capabilities can be used to form radiation beams that null out the directions of high interference.

In general, the different cancellation techniques described above may need to be combined in order to achieve the intended suppression levels and, depending on the particular case, they may include the use of circulators, shielding, and other techniques. Section Sec. VII of this paper details technologies that are expected to play a significant role in future developments, especially for large bandwidth applications.

2) Standardization Efforts

FD radios have been operating in niche markets under very specific conditions; this is the case, for example, of gap-fillers for coverage extension in digital terrestrial television single-frequency networks [22]. Standards such as the European DVB-T/T2 and, more recently, ATSC 3.0, enable the simultaneous use of the same frequency band for both transmission and reception by certain radio equipment. Other than that, standards have not openly embraced a technology with potential implementation issues, despite the promising spectral efficiency gains.

3GPP considered an early adoption of FD technology in the first standardization efforts of integrated access and backhaul (IAB) a decade ago. IAB makes it possible for operators to use their available 5G spectrum for backhaul as well as for radio access [23], [24], and has been part of the different releases since then. New modifications have been considered in Release 18, which includes a Study Item (SI) on FD operation [25]. The study presents feasibility and performance results of the so-called subband non-overlapping full duplex (SBFD) (a concept equivalent to OBFD) and dynamic/flexible TDD, along with the associated regulatory aspects. In this scenario, high passive isolation values can be achieved thanks to the use of different array panels for transmission and reception at the base station, in addition to the use of adjacent non-overlapping frequency channels. Spatial isolation within the 60–80 dB range is typically assumed by most participating partners; additionally, up to 45 dB can be achieved thanks to frequency separation, providing between 105 and 125 dB of overall passive isolation. Most companies identified the required total isolation to be in the range of 150–160 dB, so these values are only possible by incorporating active SIC and/or beam nulling. A work item in Release 19 has been approved to specify the 3GPP operation at the base station [11].

D. Full-Duplex in SatCom Domain

The principal difficulty in any FD system resides in successfully mitigating the self-interference caused by the TX into the RX. Self-interference occurs typically due to leakage between the TX and RX in the radio circuitry and antennas, as well as to back reflections from the nearby environment [10]. SI levels are expected to be particularly high in SatCom systems, due to the power imbalance between the TX and RX signals. Considering the long propagation distances of satellite links, the RX signal reaches the device very attenuated, so that the SI generated by the TX is likely to be much stronger than the desired RX signal. Another characteristic of SatCom signals with relevance to FD operation is their large fractional bandwidth, as SIC implementation increases in difficulty with the bandwidth of the links involved [26].

As discussed in Sec. II-C, mitigating SI is a difficult problem requiring the combination of different passive and active techniques acting across a number of domains (propagation, analog, and/or digital). Additionally, satellite platforms are very limited in terms of size, weight and power: even small additions to on-board equipment will result in increased size and weight, with a significant impact on launching costs. In terms of power consumption, although connected to solar panels during daylight, on-board batteries are limited and shared by multiple satellite subsystems (i.e., communication, but also propulsion, attitude and orbit control, telemetry, etc). A similar situation is found at the UE side, where cost shall be kept as low as possible. Due to these constraints, the task of SI cancellation in SatCom systems can be anticipated to be extremely challenging.

One of the early works in this area is the DoubleTalk® C-band echo canceler described in [20], which applies digital cancellation at the user terminal to attenuate the SI. However, in this specific SatCom system the signal that is transmitted and the signal that is expected at reception show similar powers levels, which significantly alleviates SIC requirements; in contrast, in many situations of interest the transmitted signal power may be significantly above in terms of power level with respect to the received signal of interest, as will be discussed in the forthcoming sections. Another early work is [27], which presents a feasibility study considering a simplified GEO satellite system operating in Ka-band. In [28], the authors study the use of additional maritime Very High Frequency (VHF) channels for VHF data exchange, with a focus on FD and HD comparison at the satellite. The bandwidth was limited to few tens of KHz and the study was carried out for LEO. The work in [29] presented results for an in-lab FD SatCom testbed, reporting a total cancellation of 105 dB. In [30], an FD feasibility analysis for inter-satellite links was presented, focusing on nano-satellites and with a central frequency of 2.4 GHz. In this context, the desired SIC level was set around 110-130 dB (distance dependent), whereas the authors achieve 80 dB in simulation and 60 dB in measurement (and assuming orthogonal linear polarization between TX and RX).

This work is licensed under a Creative Commons Attribution 4.0 License. For more information, see https://creativecommons.org/licenses/by/4.0/

This article has been accepted for publication in IEEE Open Journal of the Communications Society. This is the author's version which has not been fully edited and content may change prior to final publication. Citation information: DOI 10.1109/OJCOMS.2025.3552727

Subsection	Use Case
III.A	GEO Ka-band User Backhauling Link
III.B	LEO User Link • Hand-held access S-band • Backhauling Ka-band • Advanced-RX Ku-band
III.C	GEO Q/V-band Feeder Link LEO Q/V-band Feeder Link
III.D	GEO Ku-band TT&C Link
III.E	GEO Ka-band Feeder & User Link
III.F	LEO Ka-band Inter-Satellite Links
III.G	Ka-band Multi-Orbit Inter-Satellite Links
III.H	GEO Satellite-Terrestrial Backhauling Ka-band
III.I	Satellite - Aerial - Terrestrial links

TABLE 1. SatCom Use Cases

Frequency Band	Frequency Range
S-Band User DL	2 GHz (Time-Division Duplex TDD)
S-Band User UL	2 GHz (Time-Division Duplex TDD)
Ku-Band User DL	10.7 GHz – 12.7 GHz
Ku-Band User UL	14 GHz – 14.5 GHz
Ka-Band User DL	17.7 GHz – 20.2 GHz
Ka-Band User UL	27.5 GHz – 30 GHz
Q/V-Band User DL	37.5 GHz – 38.3 GHz
Q/V-Band User UL	47.2 GHz – 50.2 GHz; and 50.4 GHz – 51.4 GHz.

TABLE 2. SatCom Spectral Bands

Notwithstanding these previous works on SatCom domain FD, it is of interest to carry out a comprehensive evaluation of FD feasibility over a broad spectrum of SatCom use cases, including a number of frequency bands, SatCom services, bandwidth of operation, etc., in order to point out potential gains, describe current limitations, and identify novel technologies that could move FD to practical and operational systems in the future.

III. SatCom FD Use Cases

We consider a series of SatCom use cases for which FD operation may be attractive in terms of spectral efficiency gain. We have aimed at keeping this initial selection wide open, including not only feeder and user links, but also Telemetry, Tracking, and Command (TT&C) links. The use cases considered are listed in Table 1, and the corresponding system models and parameterizations are discussed in subsequent sections. Note that the actual FD feasibility analysis is presented in Section IV, while herein we focus on providing parameters and typical link budgets for HD operation, which will serve as benchmarks for the FD case. The spectrum bands under consideration in these use cases are summarized in Table 2. Additionally, inter-satellite links are assumed to operate at 26 GHz [31].

Parameter	GEO User DL (Ka-Band)
Carrier Frequency	19 GHz
Carrier Bandwidth	[56, 100, 200] MHz
Slant Range	35 786 000 m
EIRPSD	-27 [dBW/Hz] in beam center [32]
Avg. Satellite Beam Gain at Beam Center	44.4 dBi [32]
Free Space Path Loss	209.1 dB
UE Gain	39.75 dBi (VSAT 0.6 m as example [32])
UE Antenna Noise Temp.	50 K [32]
Reference Temp.	290 K [32]
Noise Figure	2.278 dB [32]
Boltzmann Constant	1.3806503e-23 J/K
Noise Power at UE	3.4517e-21 × (Carrier Bandwidth in Hz) [W]
SNR in normal operation	7.9 dB

TABLE 3. GEO user DL budget parameters (UE VSAT assumed)

Parameter	GEO User UL (Ka-Band)
Carrier Frequency	30 GHz
Carrier Bandwidth	7 MHz [33]
Slant Range	35 786 000 m
UE Tx. Power	3 dBW (VSAT assumed [34])
UE Tx. Antenna Gain	43.2 dBi (VSAT assumed [34])
Avg. Satellite Rx. Gain	51 dBi [33]
Free Space Path Loss	213 dB
Noise Power at Satellite Rx	−131.78 dBW [33]
SNR in normal operation	15.9 dB

TABLE 4. GEO user UL budget parameters (UE VSAT assumed)

A. GEO Ka-band User Backhauling Link

Most cellular base stations are connected by fiber or microwave links to the core of the network. However, in mountainous regions, low-density villages, or for remote locations, the economics of investing in this infrastructure are risky. Geostationary (GEO) satellites offer an excellent alternative to mobile backhaul service – from a single site to multi-tower aggregation. General link budget parameters for GEO user downlink (DL) and uplink (UL) are collected in Table 3 and Table 4, respectively. The typical slant range considered is 35 786 km. Since we are dealing with long propagation distances and high frequency bands, a very-small-aperture terminal (VSAT) is commonly considered, which provides enough antenna gain to close the link. It is seen from Tables 3 and 4 that the expected Signal-to-Noise Ratio (SNR) for GEO Ka-band backhauling link is 7.9 dB for the downlink, and 15.9 dB for the uplink.

B. LEO User Link

Assuming a Low-Earth Orbit (LEO) satellite, the typical slant ranges considered are 600 km or 1200 km [35]. Different parameter sets recommended by 3GPP Technical Specification Group Radio Access Network to study NTNs are provided in [35], and are considered as the baseline for this work. These include **backhauling** (high-data rate)

This work is licensed under a Creative Commons Attribution 4.0 License. For more information, see https://creativecommons.org/licenses/by/4.0/

This article has been accepted for publication in IEEE Open Journal of the Communications Society. This is the author's version which has not been fully edited and content may change prior to final publication. Citation information: DOI 10.1109/OJCOMS.2025.3552727

	LEO User DL (Ka-Band)	
Parameter	LEO-1200	LEO-600
Carrier Frequency	20 GHz	
Carrier Bandwidth	[56, 100, 200] MHz	
Slant Range	1200 km	600 km
Satellite EIRPSD	−58 dBW/Hz [35]	−64 dBW/Hz [35]
Satellite TX Beam Gain	38.5 dBi [35]	
Free Space Path Loss	180.1 dB	174.0 dB
UE Gain	39.75 dBi (VSAT 0.6 m as example [32])	
UE Antenna Noise Temp.	50 K [32]	
Reference Temp.	290 K [32]	
Noise Figure	2.278 dB [32]	
Boltzmann Constant	1.3806503e-23 J/K	
Noise Power at UE	3.4517e-21 × (Carrier Bandwidth in Hz) [W]	
SNR in normal operation	6.34 dB	6.36 dB

TABLE 5. LEO user DL budget parameters (Ka-band)

	LEO User UL (Ka-Band)	
Parameter	LEO-1200	LEO-600
Carrier Frequency	30 GHz	
Carrier Bandwidth	7 MHz [32]	
Slant Range	1200 km	600 km
UE EIRPSD	−39.82 dBW/Hz	
UE EIRP	28.63 dBW	
Free Space Path Loss	183.6 dB	177.6 dB
Satellite RX Gain	38.5 dBi [35]	
G/T Satellite	13 dB/K [34], [35]	
Noise Power at Satellite RX	−134.65 dBW	
SNR in normal operation	18.2 dB	24.2 dB

TABLE 6. LEO user UL budget parameters (Ka-band)

applications, with Ka-band spectrum and dish-type UE with mechanical steering; and **direct-to-handheld access** applications, with spectrum typically allocated in S-band (i.e., 2 GHz). Despite the recommendations of 3GPP [35], most of the current operational LEO constellations work on the spectrum at Ku-band (i.e., 12 GHz)[1], in which case the UE is assumed to be equipped with some antenna architecture with beamforming capability or mechanical steering to be able to track the satellite (e.g., a planar array).

Table 5 shows a general LEO user downlink budget parameterization for Ka-band (thus assuming dish-type UE). Typical values of SNR for LEO user DL are indicated in the last row of Table 5, i.e., SNR = 6.34 dB for LEO at 1200 km, and SNR = 6.36 dB for LEO at 600 km.

Similarly, Table 6 shows a general LEO user uplink budget parameterization for Ka-band (thus assuming VSAT-type UE). Note that 3GPP states in [35] an overall system

[1]This is mainly because these constellations are not designed to be compliant with the 5G NR standard (at least as of now).

Terminal	EIRP [dBm]	RX Gain [dB]	Noise Fig. [dB]	G/T [dB/K]
$UE_{ref.1}$	23	0	7	−31.6
$UE_{ref,2}$	23	0	4	−28.6
$UE_{worst_{case}}$	23	−5.5	9	−39.1
$UE_{SatPhone}$	31	3.5	3	−24

TABLE 7. Handheld terminal characteristics

	LEO User DL (S-Band)	
Parameter	LEO-1200	LEO-600
Carrier Frequency	2 GHz	
Carrier Bandwidth	30 MHz [36]	
Slant Range	1200 km	600 km
Satellite EIRPSD	−20 dBW/Hz [35]	−26 dBW/Hz [35]
Satellite TX Beam Gain	30 dBi [35]	
Free Space Path Loss	160.1 dB	154.0 dB
UE G/T	−31.6 dB/K [36] [see $UE_{ref.1}$ in Table 7]	
UE RX Gain	0 dB [36] [see $UE_{ref.1}$ in Table 7]	
SNR in normal operation	17 dB	17 dB

TABLE 8. LEO user DL budget parameters (S-band)

bandwidth of 400 MHz (Ka-band). However, the channel bandwidth has to be calculated by taking the 400 MHz system bandwidth and dividing it according to the frequency reuse factor. The bandwidth parameter can therefore vary, depending on the design. Regarding the EIRP of VSAT UE, 3GPP states in [35] a value of 46.2 dBW which, according to multiple references, e.g., [34], [36], seems to refer to the system bandwidth of 400 MHz. Considering these numbers and assumptions, an EIRPSD of 46.2 dBW / 400 MHz = 20.2 dBW/MHz = −39.8 dBW/Hz has been assumed. Table 6 shows the uplink SNR achieved assuming 7 MHz bandwidth (although the values of SNR would not vary by changing the bandwidth, because the EIRP adapts to such changes to maintain a constant SNR).

Regarding the **direct-to-handheld access** applications in S-band, several types of handheld terminals exist, each with different characteristics. Table 7, extracted from [37], shows a summary of the main handheld types, including a commercial smartphone with improved noise figure (see $UE_{ref,2}$) and a satellite-specific handheld with improved EIRP and G/T (see $UE_{SatPhone}$).

Table 8 shows a general LEO user downlink budget parameterization for S-band (thus assuming a handheld-based UE). The carrier frequency is now 2 GHz, both for downlink and uplink since TDD is conventionally assumed. A 17-dB SNR is obtained for the LEO user downlink in S-band.

Similarly, Table 9 shows a general LEO user uplink budget parametrization for S-band considering a conventional handheld terminal (see $UE_{ref.1}$ in Table 7). As expected, the uplink exhibits a poor SNR for this class of UE terminals.

This work is licensed under a Creative Commons Attribution 4.0 License. For more information, see https://creativecommons.org/licenses/by/4.0/

This article has been accepted for publication in IEEE Open Journal of the Communications Society. This is the author's version which has not been fully edited and content may change prior to final publication. Citation information: DOI 10.1109/OJCOMS.2025.3552727

Parameter	LEO User UL (S-Band)	
	LEO-1200	LEO-600
Carrier Frequency	2 GHz	
Carrier Bandwidth	30 MHz [36]	
Slant Range	1200 km	600 km
UE EIRP	−7 dBW [35][see $UE_{ref,1}$ in Table 7]	
	1 dBW for $UE_{SatPhone}$	
UE Tx. Antenna Gain	0 dB for $UE_{ref,1}$ [35], [36]	
	3.5 dB for $UE_{SatPhone}$	
Free Space Path Loss	160.1 dB	154.0 dB
Satellite Rx. Gain	30 dBi [35]	
G/T Satellite	1.1 dB/K [35]	
SNR in normal operation	−12.1 dB for $UE_{ref,1}$	-6.1 dB for $UE_{ref,1}$
SNR in normal operation	−4.1 dB for $UE_{SatPhone}$	1.2 dB for $UE_{SatPhone}$

TABLE 9. LEO user UL budget parameters (S-band)

Parameter	LEO Link Budget (Ku-Band)	
	UL	DL
Carrier Frequency	14.25 GHz	12.575 GHz [40]
Carrier Bandwidth	20 MHz [42]	125 MHz [41]
Free Space Path Loss	-177.1 dB	-176.0 dB
Gain	38.4 dB dBi (TX-UE) [42] 24.5 dBi (RX-Sat) [41]	24.5 dBi (TX-Sat) [41] 36.0 dBi (RX-UE) [42]
EIRP (dBW)	33.6 dBW [42]	34.6 dBW (satellite) [40]
G/T (dB/K)	-1 dB/K (satellite) [43]	12.2 dB/K (UE) [42]
SNR normal operation	4.8 dB	18.5 dB

TABLE 10. LEO link budget parameters (Ku-band)

On the other hand, the figures become more reasonable when a satellite-specific handheld terminal is assumed.

Finally, based on the most popular LEO constellation deployments, we provide the system parameters for the user link at Ku-band. The UE antenna architecture of such systems ranges from planar arrays, as Starlink antenna products [38], to low-profile dish antennas, such as the ones of Eutelsat-OneWeb [39]. Note that Eutelsat-OneWeb satellites orbit at 1200 km [40], thus requiring higher antenna gain to close the link than Starlink systems, whose orbits are lower. Focusing on the 1200 km orbit, Table 10 presents the parameterization of the Ku-band LEO user link. The figures therein have been taken mostly from OneWeb LEO constellation references [40], [41]. The UE RX antenna is assumed as in [42].

C. GEO/LEO Q/V-band Feeder Link

Feeder links are expected to be deployed in Q/V-band, due to the expected increase of user link transmissions in Ka-band. Moreover, the Q/V-band feeder link allocation allows locating the gateways (GWs) within the service area minimizing the interference between the feeder and user links. The frequency allocation for the feeder link in Q/V-band is provided in Table 11 [44]. In particular, up to 4 GHz are available for the uplink (where typically aggregated amounts of traffic need to be dealt with). Considering 2 polarizations, an overall bandwidth of 8 GHz is available.

Feeder link DL	Feeder link UL
37.5–38.3 GHz	47.2–50.2 GHz 50.4–51.4 GHz

TABLE 11. Feeder Link Frequency of Operation Q/V-band [44]

The main drawback of having feeder links operate in Q/V-band is the high sensitivity to weather impairments. As noted in [45], heavy rain attenuation can cause a loss of the order of 15-20 dB. Scintillations are also more pronounced in Q/V-band with respect to Ka-band, with typical scintillations varying around 2 dB [46]. Uplink power control may partly compensate for this loss, although the common approach is to have GW diversity, i.e., deploying multiple GWs in different geographical locations to increase the probability of link availability [45].

Tables 12 and 13 show the link budget parameters considered for Q/V-band feeder uplink, respectively for the GEO and LEO scenarios. The data therein have been extracted from [47, p. 32]. Although [47, p. 32] provides data for LEO altitudes of 1350 km and 10 355 km, we kept only the figures related to the former, which is more in-line with current LEO constellations.

Parameter	Feeder Link (Q/V-band) - GEO	
	UL	DL
Carrier Frequency	50.2 GHz	38.5 GHz
Bandwidth	2 GHz	300 MHz
Free Space Path Loss	217.5 dB	215.2 dB
Gain	59.7 dBi (TX-GW) 53 dBi (RX-Sat)	53 dBi (TX-Sat) 57.8 dBi (RX-GW)
EIRP (dBW)	80	66.4
G/T (dB/K)	24.4	32.4
SNR normal operation	22.5 dB	27.4 dB

TABLE 12. GEO parameters for feeder link [47, p. 32]

Parameter	Feeder Link (Q/V-Band) - LEO	
	UL	DL
Carrier Frequency	50.2 GHz	38.5 GHz
Bandwidth	2 GHz	300 MHz
Free Space Path Loss	189.1 dB (LEO-1350)	186.8 dB (LEO-1350)
Gain	49.3 dBi (TX-GW) 40.6 dBi (RX-Sat)	40.6 dBi (TX-Sat) 47.3 dBi (RX-GW)
EIRP (dBW)	50.5	33.9
G/T (dB/K)	10.5	19.3
SNR normal operation	7.5 dB	10.3 dB

TABLE 13. LEO parameters for feeder link [47, p. 32]

This work is licensed under a Creative Commons Attribution 4.0 License. For more information, see https://creativecommons.org/licenses/by/4.0/

This article has been accepted for publication in IEEE Open Journal of the Communications Society. This is the author's version which has not been fully edited and content may change prior to final publication. Citation information: DOI 10.1109/OJCOMS.2025.3552727

	GEO TT&C (Ku-band)	
Parameter	**UL**	**DL**
Carrier Frequency	14.5 GHz	12.2 GHz
Carrier Bandwidth	[32, 128] kHz [50]	
Slant Range	35 786 000 m	
EIRP	68 dBW (Earth Station)	5 dBW (Satellite)
Free Space Path Loss	206.8 dB	205.3 dB
Gain at RX	25 dB (Satellite)	60.01 dB (Earth Station)
G/T	0.0 dB/K [51]	37.5 dB/K (Earth Station)
SNR in normal operation	38.8 dB	14.8 dB

TABLE 14. GEO TT&C link budget parameters in Ku-band

Feeder Link (Ka-band) - GEO		
Parameter	**UL**	**DL**
Carrier Frequency	30 GHz	20 GHz
Bandwidth	2 GHz	300 MHz
Free Space Path Loss	-209.5 dB	-213.1 dB
Gain	57.5 dBi (TX-GW) 49 dBi (RX-Sat)	49 dBi (TX-Sat) 54 dBi (RX-GW)
EIRP (dBW)	72.5 (GW)	65 (Satellite)
G/T (dB/K)	20 (satellite)	31.5 (GW)
SNR normal operation	15.0 dB	30.8 dB

TABLE 15. GEO Parameters for feeder link in Ka-band ([47] page 16)

D. GEO Ku-band TT&C Link

TT&C is a critical spacecraft function ensuring correct operation of the flying system [48]. Since commands are simple data that trigger specific spacecraft actions, *telecommand* data (ground-to-space) rates are usually in the order of some Kbps (or even bps). *Telemetry* data (space-to-ground) refers to the monitoring of the spacecraft and typically is also in the order of some kbps or a few Mbps. On the other hand, *tracking* is the function related to the spacecraft's flight dynamics (two-way communication link). Even if the required data rate for TT&C is not high, it is crucial that TT&C signals be reliably received and without interruption.

The unique propagation characteristics of C-band make it an excellent candidate for TT&C. However, the overcrowded spectrum at C-band is causing many operators to move TT&C links to higher spectral bands, such as Ku-band. We shall focus on Ku-band in this use case, as it is envisaged to be used for TT&C operation of future missions. The link budget parameters for TT&C links deployed at Ku-band are summarized in Table 14, where most of the data therein have been extracted from [49], [50].

The data from USASAT-24K in [49, Tables 6 & 8] have been considered for the uplink and downlink, which are deployed between 14.0–14.5 GHz and 11.7–12.2 GHz, respectively. Note that TT&C Earth Stations are generally equipped with large dishes (e.g., the dish of USASAT-24K has a diameter of 9.3 m).

E. GEO Ka-band Feeder & User Link

This use case considers the combination of the user links defined in Secs. III-A and III-B, and the feeder links introduced in Sec. III-C. Obviously, the same satellite orbit and frequency will be assumed for FD operation.

There are no current or near-future plans for user-links at Q/V-band. Therefore, this use case considers operation in Ka-band, where it is more likely to encounter both user and feeder links. One specific characteristic is that feeder links assume much larger transmission bandwidth than user links, as they aggregate the traffic from multiple user terminals [52].

Constellation	Starlink	OneWeb	Kepler
Total no. of satellites	1584 (*)	648	140
No. of orbital planes	72 (*)	18	7
Satellites per orbital plane N_p	22	36	20
Altitude l_s (km)	550	1200	575
Slant Range d_I (km)	1970	1320	2173
Intended Service	Broadband	Broadband	IoT

(*) Information from the planes reported on initial plans.

TABLE 16. Satellite Constellation Examples [31]

For the user link UL definition, the reader is referred to the GEO user link UL setting in Table 4. The feeder link DL is shown in Table 15, which considers Ka-band and a 3 m dish at the GW station.

For the user link DL definition, the reader is referred to the GEO user link DL setting in Table 3. The feeder link UL is shown in Table 15, which considers Ka-band and a 3 m dish at the GW station.

F. LEO Ka-band Inter-Satellite Links

Assuming evenly distributed satellites within the same orbital plane (and same altitude), the corresponding slant range between two neighboring satellite nodes can be obtained using the chord length formula of a circle:

$$d_I = 2(R_E + l_s)\sin(\pi/N_p) \tag{1}$$

where N_p is the number of satellites in the orbital plane, l_s is the satellite altitude, and R_E is the earth radius, which is approximated to 6371 km. Considering the figures provided in [31], Table 16 shows the inter-satellite link (ISL) slant range d_I for the most popular LEO constellations.

Table 17 shows a simplified parametrization of ISL links, with data extracted from [31]. The predicted SNR for ISL in Ka-band is 7.2 dB.

G. Ka-band Multi-Orbit Inter-Satellite Links

At the time of writing, ISLs between different orbits are future-term technology projections, although it may be expected that, as constellations develop, the popularity of multi-orbit satellite systems will increase (e.g. IRIS2 [53]), bringing forth a demand for inter-orbital links. Inter-orbital

This work is licensed under a Creative Commons Attribution 4.0 License. For more information, see https://creativecommons.org/licenses/by/4.0/

This article has been accepted for publication in IEEE Open Journal of the Communications Society. This is the author's version which has not been fully edited and content may change prior to final publication. Citation information: DOI 10.1109/OJCOMS.2025.3552727

Inter-Satellite Links (Ka-band)	
Carrier Frequency	26 GHz
Bandwidth	500 MHz
Free Space Path Loss	Can be calculated with slant range of Table 16
Gain	34.41 dBi (RX and TX)
EIRP	44.41 dBW
Noise power	−114.99 dBW
SNR normal operation	7.2 dB

TABLE 17. ISL Parameters [31]

ISLs can be established between LEO-MEO, LEO-GEO or MEO-GEO. The reduced distance of the LEO-MEO configuration makes this case attractive, but the relative mobility of the platforms raises significant challenges. The available literature on LEO-MEO ISL is scarce, and reduces to high-level preliminary studies which reflect the low maturity of the inter-orbital ISL technology [54]. Table 18 presents a potential scenario of LEO-MEO ISL considering the altitude of Starlink shell 1 and the MEO mPower constellation of SES. Since ISL technology is significantly more mature for single-orbit scenarios, the evaluation of required self-interference isolation carried out in Sec. IV will focus on the single-orbit ISL use case presented in Sec. III-F.

TABLE 18. Ka-band Multi-Orbit ISL

LEO Satellite	
Altitude	550 Km
MEO Satellite	
Altitude	8062 Km
LEO-LEO ISL	
Carrier Frequency	26 GHz
Bandwidth	500 MHz
Slant Range	1970 Km
LEO-MEO ISL	
Carrier Frequency	26 GHz
Bandwidth	500 MHz
Slant Range	7512 Km

H. GEO Satellite-Terrestrial Backhauling Ka-band

The most obvious application of satellite communication in a 5G delivery architecture is in the backhaul segment of the network. To improve the capacity of mobile wireless backhaul networks, the concept of a seamlessly integrated satellite–terrestrial backhaul network in the Ka-band capable of jointly exploiting the terrestrial and satellite links depending on the traffic demands has been the focus of [55], [56], where a cooperative frequency assignment approach is assumed that imperatively avoids FD operation. However, FD at the Base Station (BS) can be considered to simultaneously operate a satellite link and a terrestrial backhauling link. This use case is shown in Fig. 3, which illustrates FD operation on the satellite downlink. Table 19 provides the link budget parameterization for this use case, where data have been extracted from [33] and [55].

Satellite	GEO	
Altitude	35 786 km	
	Satellite Backhauling (Downlink)	**Satellite Backhauling (Uplink)**
EIRP	62.4 dBW (satellite)	50 dBW (VSAT)
Frequency	18.7 GHz	28.5 GHz
Bandwidth	62.5 MHz	7 MHz
Gain TX	53 dBi (satellite)	42.1 dBi (VSAT)
Gain RX	42.1 dBi (VSAT)	53 dBi (satellite)
Noise Power	−126.46 dBW (VSAT)	−131.78 dBW (satellite)
	Terrestrial Backhauling	
Distance	832.58 meters	
Frequency	18.7 GHz	
Bandwidth	56 MHz	
Transmit PSD	−38.13 dBW/MHz	
Gain TX	38 dBi	
Gain RX	38 dBi	
TX Power	−20.65 dBW	
EIRP	17.35 dBW	
Noise PSD	−139 dBW/MHz (ITU-R F.758-6)	

TABLE 19. Satellite-Terrestrial Backhauling - Link Budget Parameters

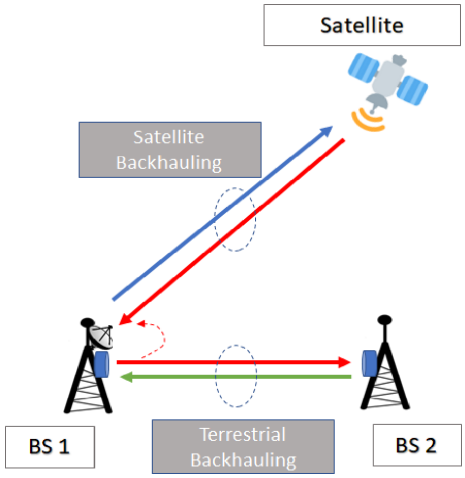

FIGURE 3. FD between a satellite backhauling link and a terrestrial backhauling link in Ka-band (red links).

I. Satellite - Aerial - Terrestrial links

Envisioned Satellite-Aerial-Terrestrial systems consider a High Altitude Platform (HAP) that supports a network of ground Internet-of-Things (IoT) nodes by relaying their data towards a satellite. In this way, a two-step uplink from ground users to the satellite is established, which is of interest since direct uplink is generally power-inefficient for battery-powered IoT devices. Furthermore, satellite backhauling can improve the flight-time of the HAP. Whereas there are a few initial studies for the GEO-HAP-UE communication (downlink), see e.g. [57], the IoT uplink remains challenging due to the power levels required to reach the HAP. For this reason, and due to the low technology readi-

This work is licensed under a Creative Commons Attribution 4.0 License. For more information, see https://creativecommons.org/licenses/by/4.0/

This article has been accepted for publication in IEEE Open Journal of the Communications Society. This is the author's version which has not been fully edited and content may change prior to final publication. Citation information: DOI 10.1109/OJCOMS.2025.3552727

ness of this use case, it was decided not to include it in the evaluation carried out in Sec. IV.

IV. Full-Duplex Feasibility Analysis

Following the 3GPP studies for FD communication [58] [59] [60], we use *receiver desensitization* as a design metric, illustrated in Fig. 4, and defined as the degradation of the Signal-to-Noise-plus-Interference Ratio (SINR) under FD operation with respect to that under HD operation. Another important metric, *TX-RX isolation* (ISO), is also illustrated in Fig. 4. It is defined as the ratio of the transmit power to self-interference power at the RX. In practice, to achieve acceptable isolation values, a combination of different strategies must be applied, as discussed in Sec. II-C.

With regard to Fig. 4, the reference noise power (dashed line) corresponds to that under HD operation. Then, under FD operation, an SI-induced component appears (solid red line), so that the overall SI-plus-noise power (dotted line) will be above the original noise floor value. The ratio between these two values equals the RX desensitization, which is always larger than 1 (i.e., always positive when expressed in dB).

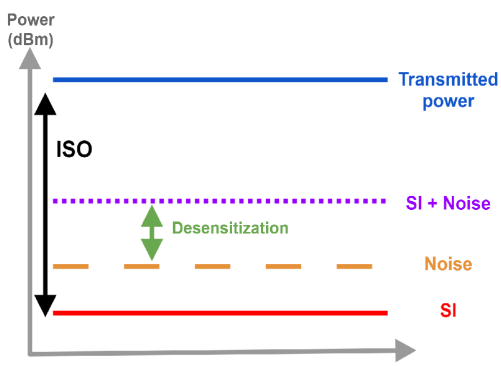

FIGURE 4. Illustration of desensitization and isolation (ISO) due to self-interference (SI).

A. Methodology

Our approach is to set a target RX desensitization value, and then find the corresponding maximum admissible SI power at the RX. With this, the required overall isolation to achieve such target desensitization and SI power will be obtained. The feasibility of each use case will be assessed by analyzing the required isolation having as reference the isolation achievable with current technology. Next we present the specific steps of this feasibility evaluation process.

Let snr denote the SNR under HD operation (in natural units), given by

$$snr = \frac{p_{SoI}}{p_{n_{RX}}}, \tag{2}$$

where p_{SoI} and $p_{n_{RX}}$ respectively denote the power of the received signal of interest and of the RX thermal noise.

Parameter	Definition
$p_{NL_{RX}}$	Non-linear terms from LNA, RX mixer and Variable Gain Amplifiers (VGAs).
$p_{NL_{PA}}$	Non-linear terms from TX power amplifier (PA)
p_{qn}	Quantization noise
$p_{n_{RX}}$	RX thermal noise
$p_{n_{TX}}$	Induced TX thermal noise
p_{IM}	Image component from RX and TX mixers

TABLE 20. List of power terms associated with non-linear effects.

Analogously, the SINR under FD operation is given by

$$sinr = \frac{p_{SoI}}{p_{n_{RX}}+p_{SI}+p_{NL_{RX}}+p_{NL_{PA}}+p_{qn}+p_{n_{TX}}+p_{IM_{RX}}+p_{IM_{TX}}}, \tag{3}$$

where p_{SI} denotes the power of the SI component, and the remaining power terms in the denominator of the right-hand side of (3), corresponding to SI-induced nonlinear distortion, are summarized in Table 20. Since one has

$$sinr = \frac{snr}{des}, \tag{4}$$

where des is the desensitization, it follows that

$$des = \frac{p_{n_{RX}}+p_{SI}+p_{NL_{RX}}+p_{NL_{PA}}+p_{qn}+p_{n_{TX}}+p_{IM_{RX}}+p_{IM_{TX}}}{p_{n_{RX}}}. \tag{5}$$

From eq. (5) it becomes evident that the performance degradation is not only caused by the residual SI, but also by the additional nonlinear terms due to hardware impairments. The isolation is finally obtained as

$$iso = \frac{p_{tx}}{p_{SI}+p_{NL_{RX}}+p_{NL_{PA}}+p_{qn}+p_{n_{TX}}+p_{IM_{RX}}+p_{IM_{TX}}}, \tag{6}$$

where p_{tx} is the transmit power of the FD node. The exact power term expressions employed for the required isolation computations are presented in the Appendix A.

B. Feasibility Results

As a first step, we consider a favorable setting in which SI-induced nonlinear distortion is assumed absent. In this way, (3), (5) and (6) reduce to

$$sinr = \frac{p_{SoI}}{p_{n_{RX}}+p_{SI}}, \quad des = 1+\frac{p_{SI}}{p_{n_{RX}}}, \quad iso = \frac{p_{tx}}{p_{SI}}. \tag{7}$$

The motivation is to quickly identify those use cases with very demanding requirements even under these benign conditions. A more refined analysis including nonlinear distortion terms will be presented in turn in Sec. VI only for the most promising use cases, for the sake of clarity and space.

Considering a target desensitization value of 1 dB, the required isolation was initially computed for all use cases under scrutiny, as shown in Table 21. It shall be noted that we evaluated two FD modes, denoted as Multi-Beam (MB) and Single-Beam (SB), and illustrated in Fig. 5 for clarity. In particular, the MB mode only requires SIC on-board the satellite (denoted as SIC-1 in Fig. 5 and Table 21), while the SB mode needs SIC on-board as well as on-ground (denoted as SIC-2 in Fig. 5 and Table 21). Note that the use case of FD

This work is licensed under a Creative Commons Attribution 4.0 License. For more information, see https://creativecommons.org/licenses/by/4.0/

This article has been accepted for publication in IEEE Open Journal of the Communications Society. This is the author's version which has not been fully edited and content may change prior to final publication. Citation information: DOI 10.1109/OJCOMS.2025.3552727

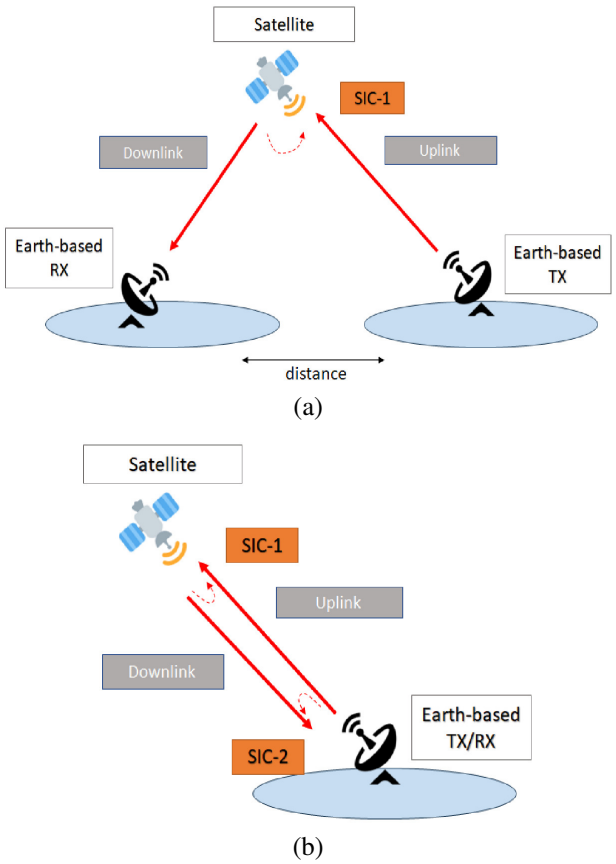

FIGURE 5. Evaluated FD modes: (a) Multi-Beam (MB), (b) Single-Beam (SB). SIC-1 and SIC-2 operate on-board and on-ground, respectively.

between feeder and user links described in Sec. III-E always considers different Earth stations for the uplink and for the downlink, thus only SIC-1 is presented in Table 21 for this use case. Similarly for the satellite-terrestrial backhauling case presented in Sec. III-H, which only requires SIC-2. Note that the user-feeder link FD can distinguish two cases: (i) FD in uplink UL and downlink FL, (ii) FD in downlink UL and uplink FL. These are indicated in Table 21 as "GEO Ka-band User Feeder Link Case 1" and "GEO Ka-band User Feeder Link Case 2", respectively.

The color code in Table 21 indicates promising use cases in green (good) and yellow (medium), depending on the required isolation level (i.e., the lower, the better).

For each use case considered, Table 21 also provides the so-called *Figure of Merit* (FOM) as defined in [10]:

$$FOM = 10 \cdot \log_{10}\left(iso \cdot W \cdot \frac{p_{tx}}{des}\right) \text{ [dBm·MHz]}, \quad (8)$$

where W is the bandwidth in MHz, the FD node transmit power p_{tx} is in mW, and both iso (isolation) and des (desensitization) are expressed in natural units [10]. State-of-the art FOM values for IBFD operation barely achieve 160 dB [10, Fig. 1.9], a figure which could possibly be higher if OBFD is considered by operating in adjacent bands. The required cancellation entails the interplay of several subsystems, which should be carefully integrated in practice. The high required levels of TX-RX isolation can be more practically approached in certain cases, e.g., when TX and RX antennas point at different directions.

As observed from Table 21, coloring of potential use cases is mostly based on the required SIC suppression or isolation, and the corresponding relative value of the FOM with respect to the state of the art.

Besides technical feasibility, there are other aspects to consider regarding the applicability of FD in the different use cases:

- **From the regulatory perspective:** in general, bringing FD operation to SatCom is challenging, as these systems have traditionally been FDD-based for many years (analogously, cellular terrestrial systems have been TDD-based). Still, the need for more spectrum is pushing classical multiplexing schemes towards novel and more advanced methodologies. 3GPP is already considering dynamic spectrum access as a key component for the future 6G, and the concept of Integrated Access-Backhaul (IAB) has been already standardized for terrestrial networks. Thus, an open mentality in terms of regulation will be needed for the introduction of FD in SatCom, as a number of changes will be required to accommodate simultaneous downlink and uplink access to the same spectral resources.
- **From the business perspective**, backhauling is the classical bandwidth-hungry application of SatCom [61]. In this sense, FD can be regarded as a great opportunity; and similarly for the feeder links, which are known to be in need of wide bandwidths. On the other hand, direct access is still under development [62], and the market at the moment is not large enough to motivate a strong need for FD operation; TT&C does not require large bandwidths [48], either. Optical ISL seems to be slowly taking over the role of RF ISL [63], and no spectrum shortage is foreseen for those systems.

Based on the obtained results, which are summarized in Table 22, we shortlist the following use cases for further consideration, as described in the following sections:

- LEO user link backhauling at Ka-band (assuming VSAT UE), SIC-1 only (on-board SIC).
- LEO feeder link at Q/V-band, SIC-1 only (on-board SIC).
- TT&C for GEO satellites at Ku-band, SIC-1 only (on-board SIC).
- GEO satellite-terrestrial backhauling in Ka-band, SIC-2 (on-ground SIC).

V. Antenna Passive Isolation

To assess in detail the feasibility of the four use cases shortlisted in Sec. IV-B, we first need to have a good understanding of the isolation that can be achieved from antenna-based passive techniques. This is of paramount

This work is licensed under a Creative Commons Attribution 4.0 License. For more information, see https://creativecommons.org/licenses/by/4.0/

This article has been accepted for publication in IEEE Open Journal of the Communications Society. This is the author's version which has not been fully edited and content may change prior to final publication. Citation information: DOI 10.1109/OJCOMS.2025.3552727

Use Case	SIC ID	SIC Band. [MHz]	ISO [dB]	FOM [dBm·MHz]	Carrier Freq. [GHz]
GEO Ka-Band Backhauling User Link	SIC-1	56	134.67	187.23	19
	SIC-2	7	137.29	174.96	
LEO Handheld Access User Link with $UE_{ref.1}$	SIC-1	30	149.57	212.11	2
	SIC-2	30	121.10	157.87	
LEO Handheld Access User Link with $UE_{SatPhone}$	SIC-1	30	149.57	212.11	2
	SIC-2	30	133.40	178.17	
LEO Backhauling Ka-Band User Link	SIC-1	56	114.47	143.93	20
	SIC-2	7	135.83	172.32	
LEO Advanced-RX Ku-Band User Link	SIC-1	125	138.10	198.17	12.575
	SIC-2	20	132.19	169.25	
GEO Q/V Feeder Link	SIC-1	300	134.50	201.62	38.5
	SIC-2	2000	136.36	218.67	
LEO Q/V Feeder Link	SIC-1	300	106.20	151.67	38.5
	SIC-2	2000	121.36	184.57	
GEO Ku-Band TT&C Link	SIC-1	0.125	138.40	138.47	12.2
	SIC-2	0.125	168.89	196.96	
GEO Ka-band User Feeder Link Case 1	SIC-1	300	137.30	207.07	30
GEO Ka-band User Feeder Link Case 2	SIC-1	56	134.07	186.63	30
LEO Ka-Band ISL	SIC-1	500	130.86	196.85	26
	SIC-2	500	130.86	196.85	
GEO Ka-Band Satellite-Terrestrial Backhauling	SIC-2	56	111.18	137.01	18.7

TABLE 21. Required isolation (ISO) for the different use cases. Figure of Merit (FOM) from (8). Desensitization value is set to 1 dB.

Case ID	Technical feasibility	Regulation prospect	Business oportunity
GEO Ka-Band Backhauling User Link			
LEO Handheld Access User Link with $UE_{ref.1}$			
LEO Handheld Access User Link with $UE_{SatPhone}$			
LEO Backhauling Ka-Band User Link			
LEO Advanced-RX Ku-Band User Link			
GEO Q/V Feeder Link			
LEO Q/V Feeder Link			
GEO Ku-Band TT&C Link			
GEO Ka-band User Feeder Link Case 1			
GEO Ka-band User Feeder Link Case 2			
LEO Ka-Band ISL			
GEO Ka-Band Satellite-Terrestrial Backhauling			

TABLE 22. Assessment of use cases. Green: potential viability; Yellow: potential viability with some challenges. Red: Extremely challenging, not recommended.

importance given the strict constraints in terms of size, weight, and power consumption of SatCom systems, which may bring into question the applicability of complex active (RF and/or baseband) SIC techniques. Note that three of the four use cases to evaluate (LEO backhauling at Ka-band, LEO feeder link at Q/V-band, and GEO TT&C) require high isolation values onboard the satellite, whereas for the fourth (satellite-terrestrial backhauling) the requirement is at the ground station. Next, we provide simulation results in order to assess the amount of passive isolation to be expected for on-board and on-ground antennas. In all cases, simulations were conducted in CST Microwave Studio software.

A. On-board antenna passive isolation

Consider first the scenarios in which high isolation is to be achieved on-board the satellite. Following recent trends [64], we have assumed two separated antenna arrays respectively configured for transmission and for reception. Two different approaches have been analyzed, depending on whether or not a ground plane is included between the arrays.

This work is licensed under a Creative Commons Attribution 4.0 License. For more information, see https://creativecommons.org/licenses/by/4.0/

This article has been accepted for publication in IEEE Open Journal of the Communications Society. This is the author's version which has not been fully edited and content may change prior to final publication. Citation information: DOI 10.1109/OJCOMS.2025.3552727

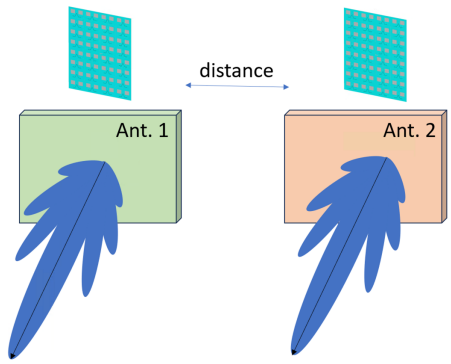

FIGURE 6. Geometry of the TX and RX phased array configuration onboard the satellite.

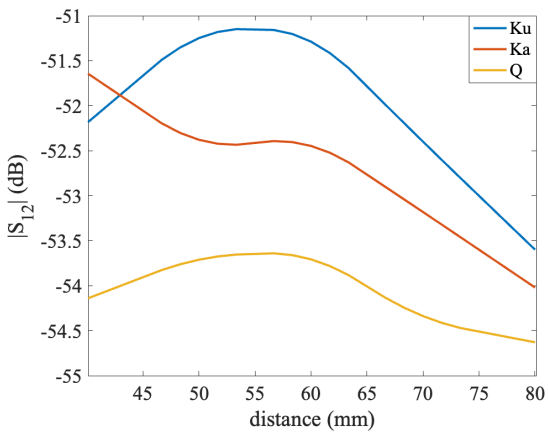

FIGURE 7. Simulation results for the configuration of Fig. 6 working at Ku-Band (11.7 GHz), Ka-Band (18.7 GHz), and Q-Band (40 GHz), using a separation between antennas in (mm).

1) Passive isolation based on antenna separation alone.

The selected array subsystems consist of 8×8 patch antennas, as illustrated in Fig. 6, with overall dimensions of approximately $5.61\lambda_0 \times 5.61\lambda_0$. Simulations were performed for three central frequencies: 11.7 GHz (Ku-band), 18.7 GHz (Ka-band), and 40 GHz (Q-band). In all cases, Rogers RO4003C substrates were used, designed for operation in linear polarization. The results, presented in Fig. 7, are analyzed in terms of inter-array separation distance expressed in millimeters, specifically within the range of 40–80 mm. It is worth mentioning that the simulation includes sampling points at five different distances. To enhance the smoothness of the curve, we applied an additional processing step. Although some natural fluctuations occur due to the electromagnetic characteristics of the antenna, we observe a general improvement in antenna isolation with increasing separation. A noticeable variation in isolation is observed between the different simulated frequencies, since the physical separation remains the same across all frequency scenarios. The highest isolation occurs in the Q-band, as the effective separation in terms of wavelengths is greater compared to the Ku- and Ka-bands.

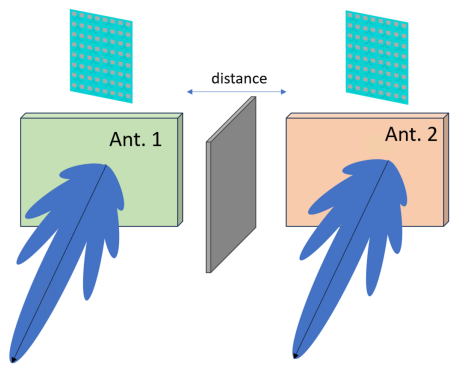

FIGURE 8. Introduction of a vertical ground plane between the phased array antennas to improve isolation.

2) Passive isolation based on antenna separation and ground plane

To further enhance the isolation between the antennas, we introduced a vertical ground plane halfway between them, as illustrated in Fig. 8, and then simulated the revised scenario. The results, shown in Fig. 9, demonstrate a significant improvement. On average, for the Ku-, Ka-, and Q-bands, the isolation improved by 24.54 dB, 21.76 dB, and 13.63 dB, respectively, for separations from 40 mm to 80 mm.

An anomaly was observed in which, for certain separations, the isolation decreased with increasing distance. This behavior can be attributed to surface currents that, at specific distances, constructively interfere, negatively affecting isolation.

However, introducing a vertical ground plane between the two antennas may affect their radiation patterns and gain, as it can introduce unwanted reflections or losses, potentially generating side lobes or nulls in certain directions. This effect is particularly noticeable in the results obtained for the Ku- and Ka-bands, where the initial separation of 40 mm is insufficient. At these frequencies, the close proximity of the ground plane alters the radiation pattern, causing deviations in the main lobe and side lobes, which ultimately enhances isolation. In contrast, this phenomenon is not observed in the Q-band, where a separation of 40 mm corresponds to approximately $6\lambda_0$, providing sufficient distance to prevent significant distortion of the radiation pattern.

B. On-ground antenna passive isolation

The use case requiring on-ground isolation corresponds to satellite-terrestrial integrated backhauling, where a VSAT terminal is receiving a signal from a GEO satellite, while a co-located drum antenna transmits toward another antenna on Earth. This scenario is illustrated in Fig. 10. In this configuration, for an antenna operating in Ka-band (27.5–30 GHz) we evaluate (i) the impact of antenna separation; (ii) the effect of the elevation angle of VSAT transmission; and (iii) the impact of considering a ground plane for improved isolation. These are detailed below.

This work is licensed under a Creative Commons Attribution 4.0 License. For more information, see https://creativecommons.org/licenses/by/4.0/

This article has been accepted for publication in IEEE Open Journal of the Communications Society. This is the author's version which has not been fully edited and content may change prior to final publication. Citation information: DOI 10.1109/OJCOMS.2025.3552727

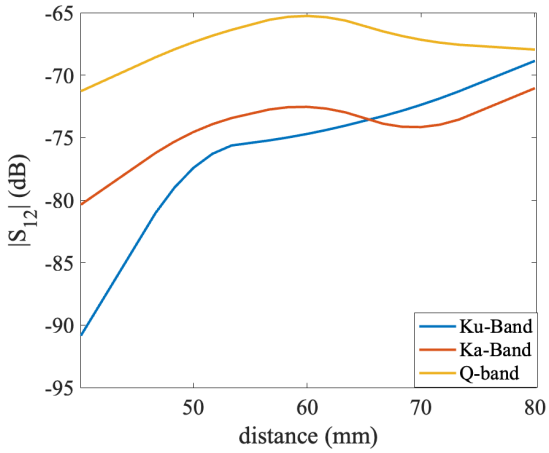

FIGURE 9. Simulation results for the configuration of Fig. 8 working at Ku-Band (11.7 GHz), Ka-Band (18.7 GHz), and Q-Band (40 GHz), using a separation between antennas in (mm).

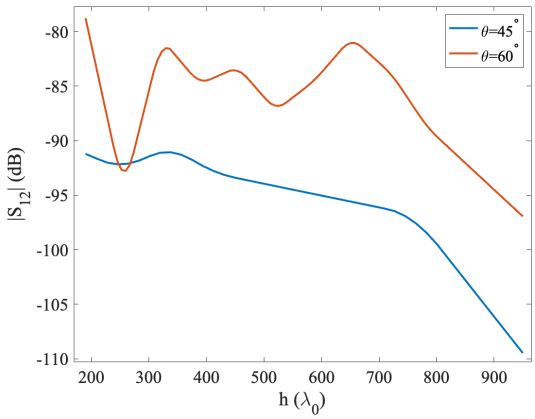

FIGURE 11. Isolation results for drum and parabolic antenna at varying heights.

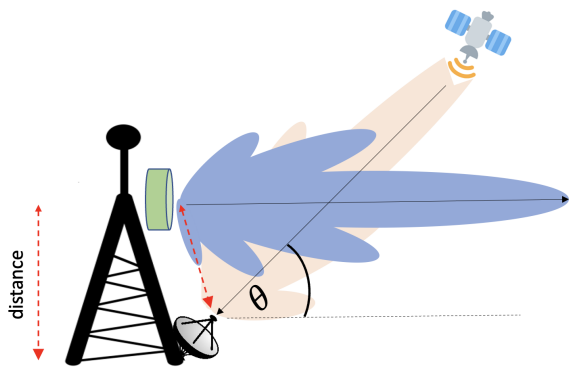

FIGURE 10. Illustration of drum and parabolic antenna separation at varying distances h.

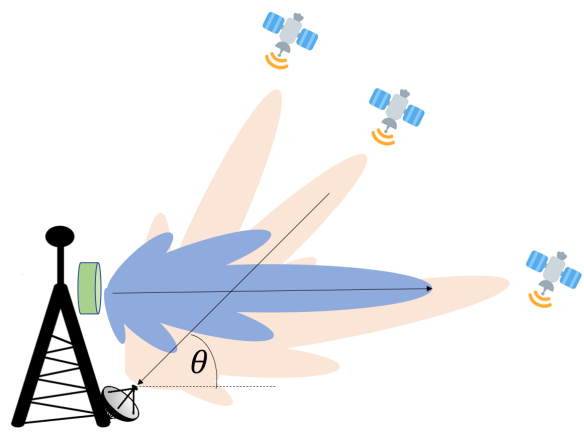

FIGURE 12. Antennas at fixed separation, with the parabolic antenna pointing at different elevation angles θ.

1) Impact of antenna separation

The apertures of the drum and parabolic antennas are 56.1 and 37.4 λ_0, respectively, both illuminated by horn antennas. The parabolic antenna is positioned at ground level, pointing at elevation angles of 45° and 60°. The height h of the drum antenna varies between 187 and 935.04 λ_0, and an operational frequency of $f_0 = 28.7$ GHz is considered.

As shown in Fig. 11, isolation does not increase monotonically with height due to the reception of a side lobe by one of the antennas at specific separation values. A closer analysis reveals that for $\theta = 60°$, the isolation is lower, which is expected as the drum antenna's illumination is approached.

Finally, the maximum isolation for both results are located at the largest separation being -109 dB for $\theta = 45°$, and -96 dB for $\theta = 60°$, which allow us to infer that a possible scenario for full-duplex is when both terminals are separated a considerable altitude and pointing away from each other as much as possible.

2) Impact of VSAT elevation angle

In this scenario, the drum antenna is placed at heights of $h = 935\ \lambda_0$ and $h = 300\ \lambda_0$ above the parabolic antenna. The parabolic antenna is adjusted to various elevation angles θ between 30° and 57.5° to connect to satellites in different orbital positions (see Fig. 12). The results are shown in Fig. 13.

It is observed that isolation improves as the height increases and as the main lobe moves away from the direction of the drum antenna, until a side lobe is reached. Since the drum antenna is positioned above the VSAT, higher elevation angles result in lower isolation. To complete the analysis, we see that in the case of $h = 300\ \lambda_0$ there is a small ripple from θ = 47.5° to θ = 57°, this variation is again caused by a side lobe that is receiving this high.

3) Impact of a ground plane between TX and RX antennas

The potential of enhancing isolation by placing a mesh grid halfway between the two antennas was also considered, as depicted in Fig. 14. In this scenario, we considered $h = 935$

This work is licensed under a Creative Commons Attribution 4.0 License. For more information, see https://creativecommons.org/licenses/by/4.0/

This article has been accepted for publication in IEEE Open Journal of the Communications Society. This is the author's version which has not been fully edited and content may change prior to final publication. Citation information: DOI 10.1109/OJCOMS.2025.3552727

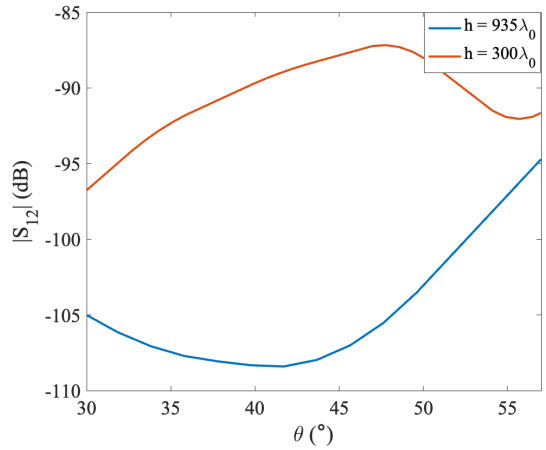

FIGURE 13. Isolation results as a function of elevation angle. Antenna separation $h = 935\ \lambda_0$ and $h = 300\ \lambda_0$.

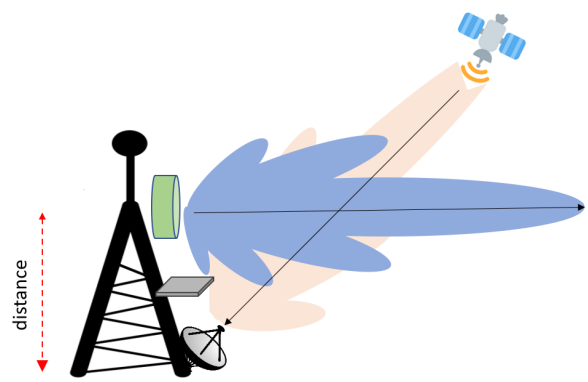

FIGURE 14. Introduction of a ground plane between the parabolic and drum antennas.

λ_0 and an elevation angle of $45°$. Simulations revealed that the introduction of the mesh grid has a negligible effect on isolation (without grid: 109.47 dB, with grid: 107.37 dB), indicating minimal effectiveness of this approach under the tested conditions. This is because both antennas are already sufficiently separated.

The isolation results for the satellite-terrestrial backhauling use case are summarized in Table 23.

VI. Detailed Analysis considering HW imperfections

We revisit now the feasibility analysis of the shortlisted use cases by considering the detrimental effect of hardware impairments and discussing approaches to achieving the required values of isolation, in view of the results from Sec. V regarding passive approaches, as well as state-of-the-art values in terms of active analog (RF) and digital (baseband) SIC. Note that the desired received signal is not only masked by the coupled transmit signal, but also by the impairments alongside [15].

Following the methodology presented in Sec.IV -A and the definitions in the Appendix A, the required isolation to achieve 1 dB of desensitization was derived. To do so, the

	Separation	Passive Isolation
w/o ground plane	$h = 935\ \lambda_0$	109.5 dB
w/ ground plane	$h = 935\ \lambda_0$	107.37 dB
	Separation	**Passive Isolation**
Worst isolation	$h = 187\ \lambda_0$	91 dB
Best isolation	$h = 935\ \lambda_0$	109.5 dB

TABLE 23. Passive isolation results for the Satellite-Terrestrial Backhauling use case (elevation $45°$).

Terrestrial Base Station in TX mode		
Parameters	Value	Notes
DAC Output power	1 dBm	To obtain the required TX PA amplification.
Mixer gain	-10 dB	To obtain the required TX PA amplification.
Mixer IRR	35 dB	Adds non-linear components due to IQ imbalance
PA TX IIP3	25 dBm	Adds non-linear components due to PA
Noise Figure	8 dB	Additional induced thermal noise due to TX
VSAT in RX mode		
Parameters	Value	Notes
LNB IRR	45 dB	Adds non-linear components due to IQ imbalance
LNB gain	55 dB	To obtain the required VGA amplification.
LNB IIP3	-30 dBm	Adds RX non-linear component
VGA IIP3	-12 dBm [a]	Adds RX non-linear component
ADC Input power	1 dBm	To obtain the required VGA amplification
Signal PAPR	10 dB	Quantization noise
ADC bit resolution	12 bits	Quantization noise

[a] Value at maximum gain, 42.5 dB

TABLE 24. On-ground SIC: Parameters related to HW imperfections.

hardware-related parameters from Table 24 for on-ground SIC, and from Table 25 for on-board SIC, were considered. They result from a comprehensive analysis of commercially available devices from RF-components vendors [65]–[74], values reported in scientific literature [75]–[79], and requirements established in relevant standards [80]. For clarity, Table 26 lists the operation frequencies for each use case, as well as the bandwidths of the signal of interest and of the self-interference.

Table 27 summarizes our findings, showing the required isolation for each selected use case assuming 1 dB desensitization. To obtain those values we adopted the following methodology:

- We compute the required isolation by following analogous steps to those described in Sec. IV-A, but taking now into account the SI-induced nonlinear terms. As can be seen, the obtained isolation requirements are a few dB more stringent than those from Table 21.
- Based on the results from Sec. V, on one hand we assume the maximum achievable value of on-board passive isolation, i.e., 75 dB, corresponding to a configuration with TX-RX array separation of 0.32 m and with insertion of a ground plane between the arrays. On the other hand, for the on-ground terminal we assume a conservative passive isolation value of 91 dB, which

This work is licensed under a Creative Commons Attribution 4.0 License. For more information, see https://creativecommons.org/licenses/by/4.0/

This article has been accepted for publication in IEEE Open Journal of the Communications Society. This is the author's version which has not been fully edited and content may change prior to final publication. Citation information: DOI 10.1109/OJCOMS.2025.3552727

On-board TX array antenna		
Parameters	Value	Notes
DAC Output power	1 dBm	To obtain the required TX PA amplification
Mixer gain	-10 dB	To obtain the required TX PA amplification
Mixer IRR	35	Adds non-linear components due to IQ imbalance
PA TX gain	22.98 dB	To obtain the required link EIRP.
PA TX IIP3	0.7 dBm	Adds non-linear components due to PA
Noise Figure	25 dB	Additional induced thermal noise due to TX
On-board RX array antenna		
Parameters	Value	Notes
Mixer IRR	35	Adds non-linear components due to IQ imbalance
Mixer gain	-10 dB	To obtain the required VGA amplification.
Mixer IIP3	20 dBm	Adds RX non-linear component
VGA IIP3	-12 dBm [a]	Adds RX non-linear component
LNA gain	20 dB	To obtain the required VGA amplification.
LNA IIP3	0 dBm	Adds non-linear components due to LNA
ADC Input power	1 dBm	To obtain the required VGA amplification
Signal PAPR	8 dB	Quantization noise
ADC bit resolution	12 bits	Quantization noise

[a] Value at maximum gain, 42.5 dB

TABLE 25. On-board SIC: Parameters related to HW imperfections.

Use Case	Band	SoI Bandwidth	SI Bandwidth
GEO Ka-Band Satellite-Terrestrial Backhauling	17.7–20.2 GHz	62.5 MHz	56 MHz
LEO Backhauling Ka-Band User Link	17.7–20.2 GHz	7 MHz	56 MHz
LEO Q/V Feeder Link	37.5–38.3 GHz	2 GHz	300 MHz
GEO Ku-Band TT&C Link	11.7–12.2 GHz	128 kHz	128 kHz

TABLE 26. Frequency band and bandwidth for the different use cases.

can be achieved with a 3-m separation between the terrestrial and satellite antennas.

- If the amount of passive isolation is below the total isolation requirement, active digital SIC is considered. As discussed in Sec. II-C, SI suppression of up to 20 dB in the digital domain seems to be reasonable based on the current literature. Note that we give preference to digital SIC over RF SIC as the latter is significantly less flexible and more complex to implement, requiring extra dedicated hardware. The reader is referred to Appendix B for the accompanying plots accounting for the interplay of digital and RF SIC in the presence of hardware impairments. The corresponding curves can be used to select an appropriate operation point.
- If the achieved isolation value considering passive and digital SIC is still insufficient, then active RF SIC becomes necessary.

The green color in Table 27 indicates feasible values (i.e., values that are deemed feasible with current technology), whereas the red color points out challenging values which would be difficult to achieve with state-of-the-art technology. It can be observed, for instance, that the satellite-terrestrial backhauling use case is perfectly feasible considering antenna-based passive isolation (91 dB) plus digital SIC (21.35 dB), without resorting to analog RF SIC. The other use cases refer to the on-board SIC for which antenna-based passive isolation is limited, so that all of them require certain

Use Case	ISO	Passive	Digital SIC	RF SIC	SE Imp.
GEO Ka-Band Satellite-Terrestrial Backhauling	112.35 dB	91 dB	21.35 dB	0 dB	87.29%
LEO Backhauling Ka-Band User Link	109.93 dB	75 dB	20.03 dB	14.9 dB	93.83%
LEO Q/V Feeder Link	106.23 dB	75 dB	20.23 dB	11 dB	90.45%
GEO Ku-Band TT&C Link	142.02 dB	75 dB	20.32 dB	46.7 dB	96.12%

TABLE 27. Summary of results for 1-dB desensitization.

Use Case	ISO	Passive	Dig. SIC	RF SIC	Des	SE Imp.
GEO Ka-Band Satellite-Terrestrial Backhauling	111 dB	91 dB	20 dB	0 dB	1.3 dB	86.28%
LEO Backhauling Ka-Band User Link	95 dB	75 dB	20 dB	0 dB	9.5 dB	41.36%
LEO Q/V Feeder Link	95 dB	75 dB	20 dB	0 dB	6.9 dB	46.31%
GEO Ku-Band TT&C Link	95 dB	75 dB	20 dB	0 dB	40.97 dB	-40.57%

TABLE 28. Summary of results without RF SIC.

amount of analog RF SIC. In particular, the LEO use cases require between 11-15 dB of RF SIC while the worst case corresponds to the GEO TT&C, which requires 46.7 dB of RF SIC.

In order to better illustrate the impact of the different domains in which SIC can be applied, we provide results for the four use cases under the following premises: (i) RF SIC is deemed too complex to implement, so that it is absent; (ii) only 20 dB of digital SIC are achievable; (iii) achievable values of passive isolation are 91 dB for on-ground and 75 dB (with ground plate separation) for on-board. These result in 111 dB of total isolation for on-ground (Satellite-Terrestrial Backhauling use case) and 95 dB for the remaining three use cases, yielding the desensitization and spectral efficiency improvement values reported in Table 28. Clearly, the on-board SIC use cases suffer significant degradation compared to the on-ground SIC use case. While the user link LEO and the feeder link LEO use cases can still achieve SE improvements of 41.36% and a 46.31% over HD operation without RF SIC, the use of RF SIC techniques become mandatory for the TT&C use case in order to obtain any SE improvement by adopting FD.

VII. Conclusions and Technological Gaps

Results from Sec. VI have evidenced that on-board SIC remains a significant challenge. The most promising and close-to-exploitation use case corresponds to the terrestrial-satellite backhauling scenario, where SIC is implemented on-ground between a VSAT RX operating at mmWave band (i.e. Ka-band) and a drum-antenna for terrestrial backhauling, both mounted in the same base station. In this scenario the TX and RX antenna elements can be strategically positioned in the base station, which greatly helps to improve passive isolation levels. This not only allows to do without any complex and costly RF SIC stages, but also relaxes the requirements on digital SIC. In addition, this scenario could be readily implemented in the near future, as it is fully compatible with current regulation, although it requires close collaboration between terrestrial and satellite operators: the digital SIC module shall connect between the baseband TX (from the terrestrial backhaul link) and the baseband RX (from the satellite VSAT receiver). Use cases considering

This work is licensed under a Creative Commons Attribution 4.0 License. For more information, see https://creativecommons.org/licenses/by/4.0/

This article has been accepted for publication in IEEE Open Journal of the Communications Society. This is the author's version which has not been fully edited and content may change prior to final publication. Citation information: DOI 10.1109/OJCOMS.2025.3552727

FD operation on-board the satellite are challenging for a number of reasons, the most critical being the moderate level of passive isolation that can be achieved due to the proximity of the TX and RX arrays. This poses strong performance requirements for the digital SIC stage. Moreover, hardware impairments and complex propagation environments may significantly affect SIC performance in general, so further evaluation in more realistic environments may be needed to confirm the conclusions above. Some considerations with practical impact can be made:

- **Multipath:** For those SatCom systems in which very small aperture terminals (VSAT) were mainly used to communicate with GEO satellites, multipath was not of significant concern. However, with the upsurge of NGSO satellites and the use of less directive antennas at the user terminal, multipath may become relevant. The presence of multipath may raise the value of SIC requirements for target residual self-interference at the RX side. This is particularly relevant to the "Satellite/Terrestrial backhauling in Ka-band" use case, for which SIC is implemented on-ground; the presence of mobile reflectors in the vicinity of the antennas (such as vehicles, wildlife, people, or wind-induced vegetation fluttering) may introduce additional multipath components in the SI channel.
- **Convergence time:** The convergence speed of digital SIC algorithms may become an issue in practice, especially in highly dynamic channel scenarios. There is a clear trade-off between convergence speed and final SIC performance.
- **Nonlinear effects:** Even though nonlinear effects were considered in the analysis, the assumptions and simplifications adopted therein may need further elaboration.
- **Passive isolation:** The feasibility analysis included a software-based evaluation of the passive isolation. However, reduced passive isolation can be experienced in practice due to unmodelled electromagnetic coupling between antenna elements.
- **Analog-to-Digital Converter (ADC) saturation:** The self-interference signal could drive the RX ADC into saturation if the characteristics of the hardware and the signal power are not carefully addressed.
- **On-board FD:** The anticipated on-board passive isolation is found to be insufficient to avoid the use of RF SIC, even with the inclusion of elements such as ground planes which increase payload weight. However, on-board RF SIC represents a formidable challenge in terms of complexity, power consumption for payloads, and the need to handle wide bandwidths and operate at high frequency bands in the microwave spectrum.
- **Regulation:** Current radio regulation imposes orthogonal uplink and downlink bands for satellite operation; hence, the adoption of on-board FD necessarily calls for changes in current standards.

The successful implementation of FD technology, at least for those scenarios aligned with the spectrum regulation, requires some additional R&D effort in high frequency RF SIC, antenna passive isolation, and SI channel modeling, among others. Using electronics, active RF cancellation is usually limited to about 30 dB under controlled laboratory conditions [81], and as much as 45 dB have been reported in some references [82]. One way of overcoming the limitations of time-domain RF cancellation is the use of microwave photonics, which allow a precise tuning of many tap delays over wider bandwidths by means of optical processing. Although performance limitations arise due to losses and noise figure, the particular application of photonic cancellation systems, based on the microwave photonics (MWP) technology, is starting to prove successful to overcome the intrinsic limitations of RF analog processing in terms of bandwidth, dynamic range, reconfigurability and latency [83]–[86]. While photonics is posed as a very promising next step for improving SIC performance, numerous challenges remain in the way toward full implementation in real products. Some of the elements that conform the SIC circuits are still on the initial development phase, so achieving a higher readiness level becomes necessary.

The results presented in this paper have been carried out assuming a 100% frequency overlap between the TX and RX channels, which can be seen as a worst case assumption. In the context of 3GPP Release 18, for instance, the concept of Sub-Band non-overlapping Full Duplex (SBFD) has been introduced in a study item, where the downlink and uplink may operate on different non-overlapping frequency sub-bands but simultaneously within the same carrier bandwidth, under the conventional TDD multiplexing scheme [1], [87]. Using non-overlapping sub-bands allows to achieve a 45 dB frequency isolation, which can be added to an antenna passive isolation (e.g. use of different array panels for transmission and reception) and together achieve between 105 and 125 dB isolation. This approach, although more conservative in terms of spectral efficiency, could offer a short-term solution in line with current trends of FD adoption by 5G standardization.

Additionally, most commercial solutions focus on the sub-6 GHz frequency range, with no practical demonstrators of RF SI cancelers operating in microwave bands (e.g., Ku/Ka). In order to limit the burden imposed on the active (both analog and digital) SIC subsystems, the passive isolation between the transmit beam and the receive radio chain must be increased for wide bandwidths and different steering directions. Proper shielding structures need to be designed alongside the antenna panels, which in the case of satellite platforms can be more challenging. Novel solutions for these isolators include, for example, the use of metamaterials [88]. Recent works have considered advanced beamforming strategies for the SI suppression at the ground-user terminal side, e.g. [89] where a joint transmit and receive beamformer has been proposed assuming users equipped with active

This work is licensed under a Creative Commons Attribution 4.0 License. For more information, see https://creativecommons.org/licenses/by/4.0/

This article has been accepted for publication in IEEE Open Journal of the Communications Society. This is the author's version which has not been fully edited and content may change prior to final publication. Citation information: DOI 10.1109/OJCOMS.2025.3552727

antennas. [90] considered circularly-polarized reflectarrays for satellite FD operation by designing orthogonal reflective polarizations for the TX and RX links.

Proper SIC design requires a good understanding and characterization of the propagation conditions of the SI channel. The geometry and antenna radiation patterns shall be well characterized, making use of field measurements to understand potential multipath effects. In this context, multi-tap SIC architectures are identified as a potential solution to improve resolution performance of single-tap SIC when facing multipath environments. Furthermore, RX antenna placement could be revised with the aim to reduce the amount of multipath. A hybrid analog-digital multitap architecture is proposed in [91] to deal with wide bandwidth and high power FD operation. More recently, the use of machine learning techniques is being considered for the digital SIC segment [92]. On top of the difficult-to-predict multipath, nonlinearities present in the TX and RX chains may become more relevant, entailing an accurate characterization of hardware components. If nonlinearities are found to have a strong impact, advanced SI signal estimation may be required. In this context, certain works such as [93] showed the performance degradation of the FD scheme under imperfect SIC by considering the so-called SI cancellation quality parameter in the achievable SINR expression.

It is worth highlighting the recent trends in research, which consider the FD operation for Integrated Sensing and Communications (ISAC) [94], [95]. In these works, the radar RX operates simultaneously while transmitting, in a FD manner. The concept of ISAC is slowly moving to SatCom domain, e.g. [96], and there is no doubt that the development of FD SatCom systems could be an enabler for SatCom ISAC. In line with the latest development of Reconfigurable Intelligent Surfaces (RIS) in the terrestrial domain, recent works such as [97] have considered the in-band FD capabilities for SatCom systems ranging from sub-6 GHz to THz bands by leveraging RIS structures.

Appendix A: Power of nonlinear terms

Next we outline the computation of the power terms from Table 20, corresponding to the SI-induced nonlinear terms due to hardware impairments at the TX and RX of the FD node. We have basically followed the approach from [98], where a more comprehensive discussion can be found.

The overall SI suppression in the FD node before the analog-to-digital converter (ADC) is denoted by α_{predig}, whereas α_{dig} denotes the remaining SI suppression in the digital domain. Additional parameters featuring in the computations below are listed in Table 29.

- Non-linear terms from LNA, RX Mixer and VGA:

$$p_{NL_{RX}} = k_{VGA} \cdot k_{MIX_{RX}} \cdot k_{LNA} \cdot (\alpha_{predig} \cdot p_{TX})^3 \times \left(\frac{1}{IIP3^2_{LNA}} + \frac{k^2_{LNA}}{IIP3^2_{MIX}} + \frac{(k_{MIX_{RX}} \cdot k_{LNA})^2}{IIP3^2_{VGA}} \right) \tag{9}$$

- Non-linear terms from TX power amplifier:

$$p_{NL_{PA}} = k_{VGA} \cdot k_{MIX_{RX}} \cdot k_{LNA} \cdot \frac{\alpha_{predig} \cdot p^3_{TX}}{IIP3^2_{PA}} \tag{10}$$

- Quantization noise:

$$p_{qn} = k_{VGA} \cdot k_{MIX_{RX}} \cdot k_{LNA} \cdot \frac{\alpha_{predig} \cdot papr \cdot p_{TX}}{3 \cdot 2^{2 \cdot bits_{ADC}}} \tag{11}$$

- Induced TX thermal noise:

$$p_{n_{TX}} = k_{VGA} \cdot k_{MIX_{RX}} \cdot k_{LNA} \cdot f_{TX} \cdot \alpha_{predig} \times k_{PA} \cdot k_{MIX_{TX}} \cdot pth \tag{12}$$

$$pth = k_{Boltz} \cdot W_{Int} \cdot 290 \cdot 1000 \tag{13}$$

- Image component from RX and TX mixers:

$$p_{IM} = k_{VGA} \cdot k_{MIX_{RX}} \cdot k_{LNA} \cdot \alpha_{predig} \cdot p_{TX} \times \left(\frac{1}{IRR_{TX}} + \frac{1}{IRR_{RX}} \right) \tag{14}$$

- RX thermal noise:

$$p_{n_{RX}} = k_{VGA} \cdot k_{MIX_{RX}} \cdot k_{LNA} \cdot p^{link}_{n_{RX}} \tag{15}$$

- Signal of Interest:

$$p_{SoI} = k_{VGA} \cdot k_{MIX_{RX}} \cdot k_{LNA} \cdot p_{RX} \tag{16}$$

- Interference signal (linear component):

$$p_{SI} = k_{VGA} \cdot k_{MIX_{RX}} \cdot k_{LNA} \cdot \alpha_{predig} \cdot \alpha_{dig} \cdot p_{TX} \tag{17}$$

The gain for the power amplifier (PA) and the variable gain amplifier (VGA) are computed as follows:

$$k_{PA} = \frac{p_{TX}}{k_{MIX_{TX}} \cdot p_{DAC}}, \tag{18}$$

$$k_{VGA} = \frac{p_{ADC}}{k_{MIX_{RX}} \cdot k_{LNA} \cdot \alpha_{predig} \cdot p_{TX}}, \tag{19}$$

where p_{TX} is the transmitted power corresponding to a given Equivalent isotropic radiated power (EIRP) from the link budget configuration. The noise $p^{link}_{n_{RX}}$ and the received power p_{RX} at the input of the RX are taken from the link budget.

Appendix B: Required SIC with HW imperfections

While the results presented in Table 27 have assumed up to 20 dB of SIC in the digital domain, in this appendix we present more comprehensive results illustrating the trade-off between analog and digital suppression, affected by the front-end imperfections. In particular, Fig. 15 presents SIC results for the Satellite-Terrestrial Backhauling use case and for several values of target desensitization, with required digital suppression in Fig. 15(a) and the overall ISO in Fig. 15(b). As an example, assuming 20 dB of SIC in the digital domain when targeting 1 dB of desensitization

This work is licensed under a Creative Commons Attribution 4.0 License. For more information, see https://creativecommons.org/licenses/by/4.0/

TX	
Parameters	Definition
p_{DAC}	DAC Output power
$k_{MIX_{TX}}$	Mixer gain
IRR_{TX}	Mixer IRR
k_{PA}	PA TX gain
$IIP3_{PA}$	PA TX IIP3
f_{TX}	Noise factor (Only TX PA)
W_{Int}	Interference signal bandwidth
RX	
Parameters	Definition
IRR_{RX}	Mixer IRR
$k_{MIX_{RX}}$	Mixer gain
$IIP3_{MIX}$	Mixer IIP3
k_{VGA}	VGA gain
$IIP3_{VGA}$	VGA IIP3
k_{LNA}	LNA gain
$IIP3_{LNA}$	LNA IIP3
p_{ADC}	ADC Input power
$papr$	Signal PAPR
$bits_{ADC}$	ADC resolution

TABLE 29. List of hardware-related parameters featuring in the computation of power terms associated with nonlinear effects.

corresponds to ≈ 112 dB of isolation and ≈ 90 dB of passive plus active RF suppression, which is essentially what was considered in Table 27. Lower values of isolation and passive plus active RF suppression can suffice if the desensitization requirement is relaxed, but this will have an impact on the achieved improvement in spectral efficiency with respect to HD operation.

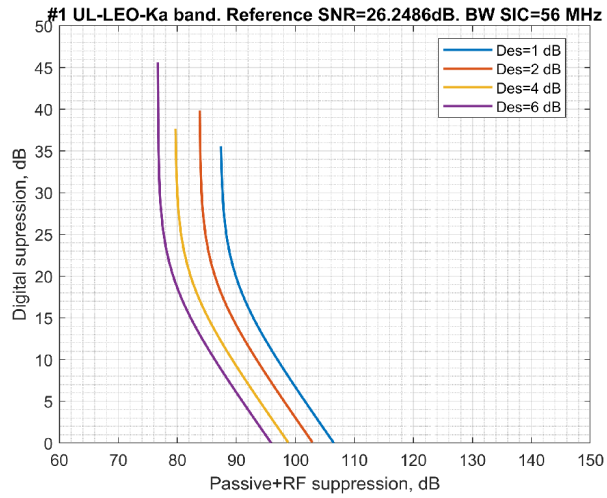

(a)

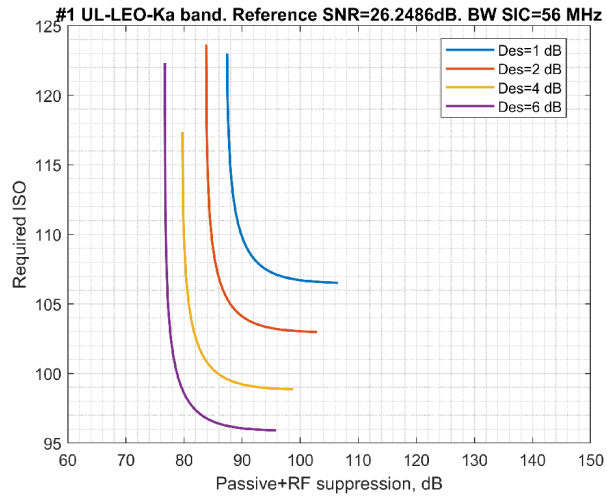

(b)

FIGURE 15. Required digital suppression and total isolation (ISO) for different values of desensitization for the LEO backhauling (Ka-band) use case. SI bandwidth is 56 MHz.

Acknowledgment

The authors would like to thank Nicolo Mazzali from ESA-ESTEC, technical officer of the ESA FDSat project, for his helpful advice and support during the activity. The authors would also like to thank the rest of Univ. of Luxembourg's team that eventually participated in the FDSat project: Juan C. Duncan, Chandan K. Sheemar, Steven Kisseleff and Victor Monzon-Baeza.

REFERENCES

[1] B. Smida, A. Sabharwal, G. Fodor, G. C. Alexandropoulos, H. A. Suraweera, and C.-B. Chae, "Full-duplex wireless for 6G: Progress brings new opportunities and challenges," *IEEE J. Sel. Areas Commun.*, vol. 41, no. 9, pp. 2729–2750, 2023.

[2] Z. Zhang, K. Long, A. V. Vasilakos, and L. Hanzo, "Full-duplex wireless communications: Challenges, solutions, and future research directions," *Proc. IEEE*, vol. 104, no. 7, pp. 1369–1409, 2016.

[3] ESA FDSat Project, "Single Channel Full Duplex Techniques for Satellite Communications," https://connectivity.esa.int/projects/esa-fdsat-project.

[4] H. Ji, Y. Kim, T. Kim, K. Muhammad, C. Tarver, M. Tonnemacher, J. Oh, B. Yu, and G. Xu, "Enabling advanced duplex in 6G," in *IEEE Int. Conf. Commun. (ICC)*, 2021, pp. 1–6.

[5] A. Sabharwal, P. Schniter, D. Guo, D. W. Bliss, S. Rangarajan, and R. Wichman, "In-band full-duplex wireless: Challenges and opportunities," *IEEE J. Sel. Areas Commun.*, vol. 32, no. 9, pp. 1637–1652, 2014.

[6] M. Duarte and A. Sabharwal, "Full-duplex wireless communications using off-the-shelf radios: Feasibility and first results," in *44th Asilomar Conf. Signals, Syst., Comput.*, 2010, pp. 1558–1562.

[7] J. I. Choi, M. Jain, K. Srinivasan, P. Levis, and S. Katti, "Achieving single channel, full duplex wireless communication," in *16th Int. Conf. Mobile Comput. Netw. (MobiCom)*, 2010.

[8] B. Smida, A. Sabharwal, G. Fodor, G. C. Alexandropoulos, H. A. Suraweera, and C.-B. Chae, "Guest editorial full duplex and its applications," *IEEE J. Sel. Areas Commun.*, vol. 41, no. 9, pp. 2725–2728, 2023.

[9] L. Laughlin, M. A. Beach, K. A. Morris, and J. L. Haine, "Electrical balance duplexing for small form factor realization of in-band full duplex," *IEEE Commun. Mag.*, vol. 53, no. 5, pp. 102–110, 2015.

[10] K. E. Kolodziej, *In-Band Full-Duplex Wireless Systems Handbook*. Artech House, 2021.

[11] M. Abdelghaffar, T. V. P. Santhappan, Y. Tokgoz, K. Mukkavilli, and T. Ji, "Subband full-duplex large-scale deployed network designs and tradeoffs," *Proc. IEEE*, vol. 112, no. 5, pp. 487–510, 2024.

[12] E. Everett, A. Sahai, and A. Sabharwal, "Passive self-interference suppression for full-duplex infrastructure nodes," *IEEE Trans. Wireless*

This work is licensed under a Creative Commons Attribution 4.0 License. For more information, see https://creativecommons.org/licenses/by/4.0/

This article has been accepted for publication in IEEE Open Journal of the Communications Society. This is the author's version which has not been fully edited and content may change prior to final publication. Citation information: DOI 10.1109/OJCOMS.2025.3552727

Commun., vol. 13, no. 2, pp. 680–694, 2014.

[13] A. Nagulu, N. Reiskarimian, T. Chen, S. Garikapati, I. Kadota, T. Dinc, S. L. Garimella, M. Kohli, A. S. Levin, G. Zussman, and H. Krishnaswamy, "Doubling down on wireless capacity: A review of integrated circuits, systems, and networks for full duplex," *Proc. IEEE*, vol. 112, no. 5, pp. 405–432, 2024.

[14] H. Alves, T. Riihonen, and H. A. Suraweera, *Full-Duplex Communications for Future Wireless Networks*. Springer, 2020.

[15] B. Smida, R. Wichman, K. E. Kolodziej, H. A. Suraweera, T. Riihonen, and A. Sabharwal, "In-band full-duplex: The physical layer," *Proc. IEEE*, vol. 112, no. 5, pp. 433–462, 2024.

[16] V. Tapio, "Full-duplex transceivers: Architectures and performance analysis," PhD thesis, University of Oulu, 2023, available at https://oulurepo.oulu.fi/bitstream/handle/10024/46657/isbn978-952-62-3919-4.pdf.

[17] C. W. Morgenstern, Y. Rong, A. Herschfelt, A. C. Molnar, A. B. Apsel, D. G. Landon, and D. W. Bliss, "Analog-domain self-interference cancellation for practical multi-tap full-duplex system: Theory, modeling, and algorithm," *IEEE J. Sel. Areas Commun.*, vol. 41, no. 9, pp. 2796–2807, 2023.

[18] 3rd Generation Partnership Project, "Technical Specification Group Radio Access Network; Study on Evolution of NR Duplex Operation (Release 18)," Tech. Rep., 12 2023.

[19] W.-S. Liao, O. Zhao, K. Li, H. Kawasaki, and T. Matsumura, "Implementation of in-band full-duplex using software defined radio with adaptive filter-based self-interference cancellation," *Future Internet*, vol. 15, no. 11, p. 360, 2023.

[20] G. D. Collins and J. Treichler, "Practical insights on full-duplex personal wireless communications gained from operational experience in the satellite environment," in *IEEE Signal Process./Signal Process. Educ. Workshop (SP/SPE)*, 2015, pp. 136–141.

[21] H. Hijazi, A. Pen, M. Le Roy, R. Lababidi, D. Le Jeune, A. Pérennec, J.-L. Issler, K. Elis, and J.-H. Corre, "Circularly polarized in-band full-duplex antenna array for Ka-band inter-cubesat links," in *20th IEEE Interreg. NEWCAS Conf. (NEWCAS)*, 2022, pp. 80–83.

[22] R. López-Valcarce, E. Antonio-Rodriguez, C. Mosquera, and F. Pérez-González, "An adaptive feedback canceller for full-duplex relays based on spectrum shaping," *IEEE J. Sel. Areas Commun.*, vol. 30, no. 8, pp. 1566–1577, 2012.

[23] G. Y. Suk, S.-M. Kim, J. Kwak, S. Hur, E. Kim, and C.-B. Chae, "Full duplex integrated access and backhaul for 5G NR: Analyses and prototype measurements," *IEEE Wireless Commun.*, vol. 29, no. 4, pp. 40–46, 2022.

[24] Y. Kim, H.-J. Moon, H. Yoo, B. Kim, K.-K. Wong, and C.-B. Chae, "A state-of-the-art survey on full-duplex network design," *Proc. IEEE*, pp. 1–24, 2024.

[25] 3GPP document TR 38.858, "Study on Evolution of NR Duplex Operation," https://portal.3gpp.org/desktopmodules/Specifications/SpecificationDetails.aspx?specificationId=3984.

[26] E. Grayver, R. Keating, and A. Parower, "Feasibility of full duplex communications for LEO satellite," in *IEEE Aerosp. Conf.*, 2015, pp. 1–8.

[27] M. R. Bhavani Shankar, G. Zheng, S. Maleki, and B. Ottersten, "Feasibility study of full-duplex relaying in satellite networks," in *IEEE 16th Int. Workshop Signal Process. Adv. Wireless Commun. (SPAWC)*, 2015, pp. 560–564.

[28] T. Ramirez and C. Mosquera, "Full-Duplex Operation in Two-Way Broadcast Service for Maritime Applications," *8th Adv. Satellite Multimedia Syst. Conf. /14th Signal Process. Space Commun. Workshop (ASMS/SPSC)*, 2016.

[29] E. Grayver, A. Parower, G. Khadge, K. Logue, and K. Tarasov, "Experimental results for a narrowband full duplex communications system," in *2017 IEEE Aerosp. Conf.*, 2017, pp. 1–10.

[30] A. Pen, M. L. Roy, R. Lababidi, D. L. Jeune, A. Perennec, J.-L. Issler, K. Elis, A. Gay, and J.-H. Corre, "Broadside FD Antenna Topologies for Nanosat Intersatellite Link," in *18th IEEE Int. New Circuits Syst. Conf. (NEWCAS)*, 2020, pp. 242–245.

[31] I. Leyva-Mayorga, B. Soret, B. Matthiesen, M. Roper, D. Wubben, A. Dekorsy, and P. Popovski, *NGSO Constellation Design for Global Connectivity*. IET, 2022, book chapter 10, pp. 237–268. [Online]. Available: https://arxiv.org/abs/2203.16597

[32] E. Lagunas, V. N. Ha, T. V. Chien, S. Andrenacci, N. Mazzali, and S. Chatzinotas, "Multicast MMSE-based precoded satellite systems: User scheduling and equivalent channel impact," in *IEEE 96th Veh. Technol. Conf. (VTC2022-Fall)*, 2022, pp. 1–6.

[33] E. Lagunas, S. K. Sharma, S. Maleki, S. Chatzinotas, and B. Ottersten, "Resource allocation for cognitive satellite communications with incumbent terrestrial networks," *IEEE Trans. Cogn. Commun. Netw.*, vol. 1, no. 3, pp. 305–317, 2015.

[34] A. Guidotti, A. Vanelli-Coralli, A. Mengali, and S. Cioni, "Non-Terrestrial Networks: Link Budget Analysis," in *IEEE Int. Conf. Commun. (ICC)*, 2020, pp. 1–6.

[35] 3GPP TR 38.821, "3rd Generation Partnership Project; Technical Specification Group Radio Access Network; Solutions for NR to support non-terrestrial networks (NTN) (Release 16)," in *V16.2.0 (2023-03)*. 3GPP, 2023.

[36] J. Sedin, L. Feltrin, and X. Lin, "Throughput and capacity evaluation of 5G new radio non-terrestrial networks with LEO satellites," in *IEEE Global Commun. Conf.*, 2020, pp. 1–6.

[37] Ginesi, Alberto, "Satellite Direct Access to Handhelds: the past, the present and the future," Keynote Speech, Nov. 2022, IPBG Instruct Project Workshop.

[38] Starlink, "Starlink planar array UT products," https://www.starlink.com/specifications.

[39] Intellian, "Eutelsat-OneWeb antenna based on Intellian products," https://www.intelliantech.com/en/products/eutelsat-oneweb/ow70l/.

[40] T. Li, J. Jin, W. Li, Z. Ren, and L. Kuang, "Research on interference avoidance effect of OneWeb satellite constellation's progressive pitch strategy," *Int. J. Satellite Commun. Networking*, vol. 39, no. 5, pp. 524–538, 2021. [Online]. Available: https://onlinelibrary.wiley.com/doi/abs/10.1002/sat.1399

[41] SatCom Guru Blog, "FCC OneWeb Filing," https://fcc.report/IBFS/SAT-MPL-20200526-00062/2379706.pdf.

[42] Intellian, "Eutelsat OneWeb dual parabolic user terminal (UT) - OW70L," https://www.intelliantech.com/en/products/eutelsat-oneweb/ow70l.

[43] SatCom Guru Blog, "OneWeb: Key Characteristics and Aero Application," https://www.satcom.guru/2016/04/oneweb-first-look-at-their-filing.html.

[44] A. Mengali, A. Ginesi, and S. D'Addio, "Computer-aided payload architecture optimization for hts satellites," in *10th Adv. Satellite Multimedia Syst. Conf. and 16th Signal Process. Space Commun. Workshop (ASMS/SPSC)*, 2020, pp. 1–8.

[45] A. Gharanjik, B. S. M. R. Rao, P.-D. Arapoglou, and B. Ottersten, "Large scale transmit diversity in Q/V band feeder link with multiple gateways," in *IEEE 24th Annual Int. Symp. Personal, Indoor, Mobile Radio Commun. (PIMRC)*, 2013, pp. 766–770.

[46] J. Ebert, W. Bailer, J. Flavio, K. Plimon, and M. Winter, "A method for ACM on Q/V-band satellite links based on artificial intelligence," in *10th Adv. Satellite Multimedia Syst. Conf. and 16th Signal Process. Space Commun. Workshop (ASMS/SPSC)*, 2020, pp. 1–5.

[47] ITU-R, "Recommendation S.1328-2: Satellite system characteristics to be considered in frequency sharing analyses between geostationary satellite orbit (GSO) and non-GSO satellite systems in the fixed satellite service (FSS) including feeder links for the mobile-satellite service (MSS)," in *ITU-R, Recommendation S.1328-2*, 2000, https://www.itu.int/dms_pubrec/itu-r/rec/s/R-REC-S.1328-2-200001-S!!PDF-E.pdf.

[48] A. Modenini and B. Ripani, "A tutorial on the tracking, telemetry, and command (TT&C) for space missions," *IEEE Commun. Surveys Tuts.*, vol. 25, no. 3, pp. 1510–1542, 2023.

[49] Rec. ITU-R S.1716, "Performance and availability objectives for fixed-satellite service telemetry, tracking and command systems," https://www.itu.int/dms_pubrec/itu-r/rec/s/R-REC-S.1716-0-200502-I!!PDF-E.pdf.

[50] B. S. Himani, K. Afzaal, K. S. Malleswar, S. Das, R. Ranjan, and M. Neelavathy, "Design of modular approach based Ku-band telemetry transmitter for geostationary satellites," in *7th Int. Conf. Commun. Syst. Netw. Technol. (CSNT)*, 2017, pp. 25–29.

[51] Fisher Telecommunications, "Link budget for a typical VSAT operation at Ku-band," https://www.fishercom.xyz/satellite-communications/a-link-budget-for-a-typical-vsat-operation-at-kuband.html.

[52] E. Lagunas, A. Perez-Neira, J. Grotz, S. Chatzinotas, and B. Ottersten, "Beam splash mitigation for NGSO spectrum coexistence between feeder and user downlink," in *26th Int. ITG Workshop Smart Antennas / 13th Conf. Syst., Commun., Coding*. VDE, 2023, pp. 1–6.

This work is licensed under a Creative Commons Attribution 4.0 License. For more information, see https://creativecommons.org/licenses/by/4.0/

[53] SpaceRise for IRIS2, "Space Consortium for a Resilient, Interconnected and Secure Europe," website, Jan. 2025, https://www.spacerise.eu/.

[54] J.-H. Hu, K. Yeung, and T. Li, "Routing and re-routing in a LEO/MEO two-tier mobile satellite communications system with inter-satellite links," in *IEEE Int. Conf. Commun. (ICC)*, vol. 1, 2000, pp. 134–138.

[55] M. Shaat, E. Lagunas, A. I. Perez-Neira, and S. Chatzinotas, "Integrated terrestrial-satellite wireless backhauling: Resource management and benefits for 5G," *IEEE Veh. Technol. Mag.*, vol. 13, no. 3, pp. 39–47, 2018.

[56] X. Artiga, A. Perez-Neira, J. Baranda, E. Lagunas, S. Chatzinotas, R. Zetik, P. Gorski, K. Ntougias, D. Perez, and G. Ziaragkas, "Shared access satellite-terrestrial reconfigurable backhaul network enabled by smart antennas at mmwave band," *IEEE Netw.*, vol. 32, no. 5, pp. 46–53, 2018.

[57] D. Wang, M. Giordani, M.-S. Alouini, and M. Zorzi, "The potential of multilayered hierarchical nonterrestrial networks for 6G: A comparative analysis among networking architectures," *IEEE Veh. Technol. Mag.*, vol. 16, no. 3, pp. 99–107, 2021.

[58] Qualcomm Inc., "R4-2302433, BS SBFD feasibility aspects," in *3GPP TSG-RAN WG4 106*. 3GPP, 2023.

[59] Ericsson, " R4-2301885, BS RF feasibility considerations ," in *3GPP TSG-RAN WG4 106*. 3GPP, 2023.

[60] Samsung, "R4-2300445, Discussion on feasibility and RF impact of SBFD: BS Aspects ," in *3GPP TSG-RAN WG4 106*. 3GPP, 2023.

[61] C. Ge *et al.*, "QoE-assured live streaming via satellite backhaul in 5G networks," *IEEE Trans. Broadcast.*, vol. 65, no. 2, pp. 381–391, 2019.

[62] F. Völk, R. T. Schwarz, and A. Knopp, "In-Lab Performance Analysis of a 5G Non-Terrestrial Network using OpenAirInterface," in *IEEE Int. Conf. Wireless for Space and Extreme Environments (WiSEE)*, 2023, pp. 167–172.

[63] J. Liang *et al.*, "Free-Space Optical (FSO) Satellite Networks Performance Analysis: Transmission Power, Latency, and Outage Probability," *IEEE Open J. Veh. Technol.*, vol. 5, pp. 244–261, 2024.

[64] Starlink SpaceX, "Satellite Technology," website, Nov. 2024, https://www.starlink.com/technology.

[65] United Monolithic Semiconductors, "Products," Online, 2024. [Online]. Available: https://www.ums-rf.com/products/

[66] Analog Devices, "Space Products Selection Guide," 2024. [Online]. Available: https://www.analog.com/media/en/news-marketing-collateral/solutions-bulletins-brochures/Space_Products_Selection_Guide.pdf

[67] Teledyne E2V, "Space-Grade ADCs/DACs," 2024. [Online]. Available: https://semiconductors.teledyne-e2v.com/en/products/space-grade-solutions/space-grade-adcs-dacs/

[68] ——, "Analog-to-Digital Converters," 2024. [Online]. Available: https://semiconductors.teledyne-e2v.com/en/products/data-converters/analog-to-digital/

[69] ——, "Digital-to-Analog Converters," 2024. [Online]. Available: https://semiconductors.teledyne-e2v.com/en/products/digital-to-analog-converters/digital-to-analog/

[70] Analog Devices, "Mixers," 2024. [Online]. Available: https://www.analog.com/en/product-category/mixers.html

[71] Teledyne Defense Electronics, "TWT Product Selection Guide," 2024. [Online]. Available: https://www.teledynedefenseelectronics.com/mec/Products/Documents/TWT%20Product%20Selection%20Guide.pdf

[72] Swedish Microwave, "LNB," 2024. [Online]. Available: https://smw.se/product-category/lnb/

[73] Orbital Research, "KA-Band LNB," 2024. [Online]. Available: https://orbitalresearch.net/products/lnb/ka-band-lnb/

[74] Norsat, "Block Upconverters (BUCs)," 2024. [Online]. Available: https://www.norsat.com/pages/bucs

[75] E. M. Suijker, M. Rodenburg, J. A. Hoogland, M. v. Heijningen, M. Seelmann-Eggebert, R. Quay, P. Bruckner, and F. E. v. Vliet, "Robust AlGaN/GaN Low Noise Amplifier MMICs for C-, Ku- and Ka-Band Space Applications," in *IEEE Compound Semicond. Integr. Circuit Symp.*, 2009, Conference Proceedings, pp. 1–4.

[76] L. Pace, P. E. Longhi, S. Fenu, W. Ciccognani, S. Colangeli, and E. Limiti, "Development of a V-Band MMIC chip-set for in-orbit Inter-Satellite Links," in *2019 Int. Symp. Adv. Electr. Commun. Technol. (ISAECT)*, 2019, Conference Proceedings, pp. 1–6.

[77] J. I. Louis, *The RF Link*. Wiley, 2017, book section 4, pp. 49–74. [Online]. Available: http://ieeexplore.ieee.org/document/8042868

[78] D. Korpi, T. Riihonen, V. Syrjälä, L. Anttila, M. Valkama, and R. Wichman, "Full-duplex transceiver system calculations: Analysis of adc and linearity challenges," *IEEE Trans. Wireless Commun.*, vol. 13, no. 7, pp. 3821–3836, 2014.

[79] P. Colantonio and R. Giofré, "A GaN-on-Si MMIC Power Amplifier with 10W Output Power and 35

[80] ETSI, "Digital Video Broadcasting (DVB); Implementation guidelines for the second generation system for Broadcasting, Interactive Services, News Gathering and other broadband satellite applications; Part 2: S2 Extensions (DVB-S2X)," Report ETSI TR 102 376-2 V1.2.1 (2021-01), 2021.

[81] V. Tapio, *Self-Interference Cancellation for Full-Duplex Transceivers*. University of Oulu, 2023, Ph.D. thesis. [Online]. Available: https://oulurepo.oulu.fi/handle/10024/46657

[82] C. W. Morgenstern, Y. Rong, A. Herschfelt, A. C. Molnar, A. B. Apsel, D. G. Landon, and D. W. Bliss, "Analog-domain self-interference cancellation for practical multi-tap full-duplex system: Theory, modeling, and algorithm," *IEEE J. Sel. Areas Commun.*, 2023.

[83] M. P. Chang, E. C. Blow, J. J. Sun, M. Z. Lu, and P. R. Prucnal, "Integrated microwave photonic circuit for self-interference cancellation," *IEEE Trans. Microw. Theory Techn.*, vol. 65, no. 11, 2017.

[84] S. Zhu, M. Li, N. H. Zhu, and W. Li, "Photonic radio frequency self-interference cancellation and harmonic down-conversion for in-band full-duplex radio-over-fiber system," *IEEE Photonics J.*, vol. 11, no. 5, 2019.

[85] A. Pandey, K. Van Gasse, and D. Van Thourhout, "Integrated photonics approach to radio-frequency self-interference cancellation," *Optics Continuum*, vol. 1, no. 9, 2022.

[86] X. Han, X. Su, M. Chao, X. Yang, W. Wang, S. Fu, Y. Du, Z. Wu, and M. Zhao, "Integrated photonic RF self-interference cancellation on a silicon platform for full-duplex communication," *Photonics Research*, vol. 11, no. 10, 2023.

[87] X. Han, R. Liu, X. Liu, C. Liang, X. Wei, Y. Hao, Z. Zhang, and S. Jin, "Interference mitigation for non-overlapping sub-band full duplex for 5G-advanced wireless networks," *IEEE Access*, vol. 10, pp. 134 512–134 524, 2022.

[88] L. N. Ribeiro, D. H. Nguyen, P. K. Gentner, and M. Göttl, "A high-isolation dual-band base station antenna design for full duplex technologies," in *2024 18th Eur. Conf. Antennas Propag. (EuCAP)*, 2024, pp. 1–5.

[89] T. Van Der Spuy, R. Maaskant, M. Ivashina, L. Nyström, and T. Eriksson, "Self-Interference Suppression for SatCom Active Antenna Arrays Through Joint Transmit and Receive Beamforming," in *European Conference on Antennas and Propagation (EuCAP)*, 2024, pp. 1–5.

[90] D. Choi and G. Byun, "Circular polarization conversion using dual frequency selective surfaces for full-duplex satellite communications," *IEEE Access*, vol. 12, pp. 120 219–120 225, 2024.

[91] Y. Liang *et al.*, "Fast estimation methods for hybrid multitap architecture in-band full-duplex transceiver with wide bandwidth and high power," *IEEE Trans. Microw. Theory Techn.*, pp. 1–14, 2025.

[92] M. Elsayed, A. A. A. El-Banna, O. A. Dobre, W. Y. Shiu, and P. Wang, "Machine learning-based self-interference cancellation for full-duplex radio: Approaches, open challenges, and future research directions," *IEEE Open J. Veh. Technol.*, vol. 5, pp. 21–47, 2024.

[93] Q. T. Ngo, K. T. Phan, W. Xiang, A. Mahmood, and J. Slay, "Two-tier cache-aided full-duplex hybrid satellite–terrestrial communication networks," *IEEE Trans. Aerosp. Electron. Syst.*, vol. 58, no. 3, pp. 1753–1765, 2022.

[94] Z. He, W. Xu, H. Shen, D. W. K. Ng, Y. C. Eldar, and X. You, "Full-duplex communication for ISAC: Joint beamforming and power optimization," *IEEE J. Sel. Areas Commun.*, vol. 41, no. 9, pp. 2920–2936, 2023.

[95] Z. Xiao and Y. Zeng, "Waveform design and performance analysis for full-duplex integrated sensing and communication," *IEEE J. Sel. Areas Commun.*, vol. 40, no. 6, pp. 1823–1837, 2022.

[96] L. Yin, Z. Liu, M. R. Bhavani Shankar, M. Alaee-Kerahroodi, and B. Clerckx, "Integrated Sensing and Communications Enabled Low Earth Orbit Satellite Systems," *IEEE Netw.*, pp. 1–1, 2024.

[97] M. Toka *et al.*, "RIS-Empowered LEO Satellite Networks for 6G: Promising Usage Scenarios and Future Directions," *IEEE Commun. Mag.*, vol. 62, no. 11, pp. 128–135, 2024.

[98] D. Korpi, *Full-Duplex Wireless: Self-interference Modeling, Digital Cancellation, and System Studies*. Tampere University of Technology,

This work is licensed under a Creative Commons Attribution 4.0 License. For more information, see https://creativecommons.org/licenses/by/4.0/

This article has been accepted for publication in IEEE Open Journal of the Communications Society. This is the author's version which has not been fully edited and content may change prior to final publication. Citation information: DOI 10.1109/OJCOMS.2025.3552727

2017, Ph.D. thesis. [Online]. Available: https://trepo.tuni.fi/handle/10024/114262

Eva Lagunas (S'09-M'13-SM'18) received the M.Sc. and Ph.D. degrees in telecommunications engineering from the Polytechnic University of Catalonia (UPC), Barcelona, Spain, in 2010 and 2014, respectively. She was Research Assistant within the Department of Signal Theory and Communications, UPC, from 2009 to 2013. In 2009 she was a guest research assistant within the Department of Information Engineering, University of Pisa, Italy. From November 2011 to May 2012 she held a visiting research appointment at the Center for Advanced Communications (CAC), Villanova University, PA, USA. In 2014, she joined the Interdisciplinary Centre for Security, Reliability and Trust (SnT), University of Luxembourg, where she currently holds a Research Scientist position. Her research interests include radio resource management and general wireless networks optimization.

Tomás Ramírez received Telecommunications Engineering degree from University of Vigo, Galicia, Spain, in 2015. He worked at the Signal Theory and Communications Department in the University of Vigo between 2015 and 2021 as an associate researcher. In 2018, he started his doctoral studies about satellite communications, focusing on new solutions in the forward link for High Throughput satellites. During his doctoral studies he collaborated in different SatNex (Satellite Network of Experts) projects, which are funded by the European Space Agency. In December 2021, he received his Ph.D. degree at University of Vigo. At the end of 2021, he joins GRADIANT technology center in the Advanced Communications Area where he currently holds the position of senior engineer-researcher. His interest focuses on satellite communications, physical layer signal design, physical layer security and in-band full duplex communications.

Juan A. Vásquez-Peralvo was born in Quito, Ecuador. He received his B. Eng. in Electronics and Telecommunications from the Escuela Politécnica Nacional, Quito, Ecuador; M.Sc. degree in Wireless Communication Systems from The University of Sheffield, Sheffield, UK; Ph.D. degree in Communication Systems from the Universidad Politécnica de Madrid, Madrid, Spain. Currently, he is pursuing a post-doc in the SIGCOM research group of the Interdisciplinary Centre for Security, Reliability, and Trust (SnT) of the University of Luxembourg, Luxembourg. His current research interests are phase array design for satellite communications, meta-surfaces, additive manufacturing, and lens antenna design.

Jorge Luis González Rios is with the Interdisciplinary Centre for Security, Reliability and Trust (SnT), University of Luxembourg. He received his B.S. Degree (with honors), M.S. Degree, and Ph.D. in Telecommunications and Electronics in 2006, 2009 and 2018, respectively, from the Technological University of Havana (CUJAE), Cuba. From September 2006 to July 2019, he was a Lecturer and Researcher with the Research Center on Microelectronics (CIME) at CUJAE. He visited the Seville Institute of Microelectronics (IMSE-CNM), Spain, in 2010, 2011, and 2012, and the Group of Microelectronics of the Federal University of Itajuba (UNIFEI), Brazil, in 2013. His research interests include RF/analog circuits, embedded systems, and wireless and satellite communications.

Pablo Losada-Sanisidro received his M.Sc. degree in Telecommunication Engineering from the University of Vigo, Spain, in 2011, where he was also awarded the End-of-Degree Award for his academic performance. From September 2009 to July 2010, he collaborated with the Signal Theory and Communications Department at the University of Vigo under a national grant for academic excellence awarded by the Spanish Ministry of Education. During this time, he participated in antenna characterization and electromagnetic compatibility certification activities at the Radioelectric Test Laboratory of the Telecommunications Engineering School in Vigo. Concurrently, he completed his bachelor's thesis at Gradiant, where he developed a direct-RF digital frequency modulator for cable applications.

Pablo has contributed to the development of high-speed signal processing algorithms on FPGAs, direct-RF digital signal sampling and synthesis hardware, and FPGA-based transceivers for both single carrier and multicarrier digital communications systems. His work spans various communication standards, including broadcast (DVB-T, DVB-C, DVB-C2, J.83B), SATCOM (proprietary waveforms), and power-line communication (PRIME 1.4 and G.hn) systems. He is currently a Technical Manager with the Electronics and Advanced Communications Department at Gradiant.

Carlos Mosquera (Senior Member, IEEE), is currently Professor at the Signal Theory and Communications Department, University of Vigo. He received the M.Sc. degree in Electrical Engineering from Stanford University, Stanford, CA, in 1994, and the Ph.D. degree in Telecommunications Engineering from University of Vigo, Vigo, Spain, in 1998. He held visiting positions with the European Space Agency, the University of New Mexico and the University of York. He was one of the promoters and Director of the Communications Area at the Galician Research and Development Center for Advanced Telecommunications (Gradiant) for five years. He was the Director of the Atlantic Research Center on Telecommunication Technologies (atlanTTic) for three years. He holds different patents in collaboration with industry, and has co-authored over 150 conference and journal papers, and two books. He has co-organized several international conferences and special sessions on communications, and is a reviewer for different European research agencies. He is member of the Satellite Network of Experts, funded by the European Space Agency, for which he has been involved in different research projects. In the field of Satellite Communications he was co-recipient of the best paper awards at several international conferences. He serves as an Associate Editor for the Frontiers in Space Technologies journal.

Roberto López-Valcarce (Senior Member, IEEE) received the telecommunication engineering degree from the University of Vigo, Spain, in 1995. During 1996 he worked for Intelsis as Project Engineer in the deployment of broadcast TV networks. He received the M.Sc. and Ph.D. degrees in electrical engineering from the University of Iowa, USA, in 1998 and 2000. He was a Post-Doctoral Fellow of the Spanish Ministry of Science and Technology from 2001 to 2006 at the University of Vigo. He is currently an Associate Professor at the Atlantic Research Center for Telecommunication Technologies, University of Vigo. From 2010 to 2013, he served as Program Manager of the Galician Regional Government R&D Program on Information and Communication Technologies. He has been the leading researcher of several publicly and privately funded R&D projects, and has co-authored over 70 papers in leading international journals, holding several patents in collaboration with industry. His main research interests include statistical signal processing, digital communications, and sensor networks.

Dr. López-Valcarce was the recipient of a 2005 Best Paper Award from the IEEE Signal Processing Society. He served as an Associate Editor of the IEEE Transactions on Signal Processing from 2008 to 2011, and as a member of the IEEE Signal Processing for Communications and Networking

This work is licensed under a Creative Commons Attribution 4.0 License. For more information, see https://creativecommons.org/licenses/by/4.0/

This article has been accepted for publication in IEEE Open Journal of the Communications Society. This is the author's version which has not been fully edited and content may change prior to final publication. Citation information: DOI 10.1109/OJCOMS.2025.3552727

Technical Committee from 2011 to 2013. Since 2018 he serves as Subject Editor for Elsevier's Signal Processing journal.

Praveen Naidu Vummadisetty (Senior Member IEEE) received PhD (2015) from Symbiosis International University, Pune, INDIA, M.Tech from DRDO – Defense Institute of Advanced Technology (DIAT) , Pune, INDIA, and B.Tech (2009) from JNTU Kakinada, Andhra Pradesh, INDIA. Currently, he is working as Postdoctoral Research Associate, SnT- SIGCOM, University of Luxembourg. He is also working as elected University Council Member for University of Luxembourg and serving as Secretary, IEEE Benelux AP/MTT Joint Chapter. Research interests are Compact Multi Band Antennas, MIMO Printed Antennas, Reconfigurable Intelligent Surface (RIS).

Symeon Chatzinotas(Fellow, IEEE) received the M.Eng. degree in telecommunications from the Aristotle University of Thessaloniki, Thessaloniki, Greece, in 2003, and the M.Sc. and Ph.D. degrees in electronic engineering from the University of Surrey, Guildford, U.K., in 2006 and 2009, respectively. He is currently a Full-Professor, and the Deputy Head of the SIGCOM Research Group, Interdisciplinary Centre for Security, Reliability, and Trust, University of Luxembourg, Esch-sur-Alzette, Luxembourg, and a Visiting Professor with the University of Parma, Parma, Italy. His research interests include multiuser information theory, cooperative/ cognitive communications, and wireless network optimization. He has been involved in numerous research and development projects with the Institute of Informatics Telecommunications, National Center for Scientific Research Demokritos, Institute of Telematics and Informatics, Center of Research and Technology Hellas, and Mobile Communications Research Group, Center of Communication Systems Research, University of Surrey. He has coauthored more than 400 technical papers in refereed international journals, conferences and scientific books. He was the co-recipient of the 2014 IEEE Distinguished Contributions to Satellite Communications Award, the CROWNCOM 2015 Best Paper Award, and the 2018 EURASIP JWCN Best Paper Award. He is currently on the Editorial Board of the IEEE Open Journal of Vehicular Technology and the International Journal of Satellite Communications and Networking.

This work is licensed under a Creative Commons Attribution 4.0 License. For more information, see https://creativecommons.org/licenses/by/4.0/